Bachelor-Arbeit

Seismic studies of the Northern Pacific mantle using full-waveforms

---

zur Erlangung des akademischen Grades

Bachelor in Erdwissenschaften

vorgelegt am Departement Erdwissenschaften der ETH Zürich

unter der Leitung von

Herr Prof. Dr. Andreas Fichtner, ETH Zürich, D-ERDW, Seismology and Wave Physics

Frau Dr. Maria Koroni, ETH Zürich, D-ERDW, Seismology and Wave Physics

---

eingereicht von

Chantal Vanessa Marti

18-932-343

am

31. July 2021, Zürich

Contents

1 Abstract

SS precursors and the ScS phase are some of the only phases that provide a good data coverage for vast areas like the Pacific Ocean. Those phases are most sensitive at the bounce point Our waveforms have been recorded by stations of the U.S. Array. Our research focuses on the 410 km and 660 km discontinuity and the core-mantle boundary (CMB). A accurate image of the Earth's interior is crucial for understanding geodynamical processes and the occurrence of earthquakes. We use full-waveform, 3D calculated synthetics and compare them to real data seismograms. This simple study is an example of how to set up seismic studies. For simplification we use only one earthquake event. We will explain how to process and prepare the real and synthetic data in Obspy, so they can be correlated. We do the correlation for the S410S, S660S and ScS phase and obtain time shifts. From there we calculate with a linearised approach the variation of the discontinuity depth. The results are stored in a database for further use. We plotted maps with the absolute depth of the discontinuity at the midpoint latitude and longitude of each trace. We found a shallower 410 km discontinuity at the Northwestern rim subduction zone of the Pacific, which is similar to other studies that we compared. For the 660 km discontinuity in the same region the depths were not really significantly different.

2 Introduction

The Earth's mantle is the area spanning from 30-80 km depth, where the Mohorovičić discontinuity occurs, separating the crust from the mantle, till the core-mantle boundary at 2891km. This area is rather complex in terms of dynamics and not homogeneous, it rather consists of many layers which are separated by discontinuities and laterally heterogeneous velocity structures. Dynamic activity inside and on the surface of the Earth such as mantle plumes and subduction zones are a result of convection and phase transitions which both cause 3-D, both laterally and vertically, heterogeneities. An important feature in the Earth is the separation between layers by interfaces which present strong velocity gradients. These are called discontinuities and act also as mantle reflectors.

Seismology provides a great tool to study these structures, since discontinuities inside the Earth are responsible for reflection, refraction and changes in velocity of seismic waves. In 1981 Dziewonski and Anderson developed the Preliminary Reference Earth Model (PREM), which is still used today as a reference model (Dziewonski & Anderson, 1981) and we also use it as our reference in this study. It is a 1-D velocity model of the Earth's interior created by using

different types of data, i.e. normal modes, surface and body waves. The model consists of four major mantle discontinuities where the velocity changes are abrupt, instead of gradual, and occur at the depths of 220 km, 410 km, 660 km and at the core-mantle boundary. The nature of these discontinuities is important because they denote changes in temperature and composition, which provide further constraints in understanding mantle dynamic processes.

In the Earth's interior, there are two well-known global discontinuities. The shallower occurs at 410 km and marks the discontinuity at the bottom of the upper mantle. Deeper down the discontinuity at 660 km marks the interface between transition zone and lower mantle. These two discontinuities define the bounds of the mantle transition zone with a thickness of approximately 250 km (Koroni & Trampert, 2021). These discontinuities are due to phase transitions in olivine which is a major mantle mineral. At 410 km olivine transitions to wadsleyite and finally the mantle mineralogy consists of perovskite and magnesiowustite at 660 km depth (Deuss, 2009), as it is illustrated in Figure 1. There are other known and reported secondary discontinuities and reflectors, namely the G-Discontinuity (60-120 km depth), the Lehmann Discontinuity (150-250 km depth), the X-Discontinuity (270-330 km depth) and speculated reflectors especially beneath subduction zone regions (Bagley & Revenaugh, 2008). The work of Bagley and Revenaugh (2008) reports the X-Discontinuity to be widespread under the Pacific region, and it is characterized by seismic velocity increase. In other studies the discontinuity was as well more pronounced under ocean basins, however it is not observed globally.

In this research project, I will focus on analysing seismic data from recorded seismograms of the US array. The selected earthquake data is located in Philippines, therefore the theoretical paths of the seismic waves under investigation are crossing the northern Pacific region. I will focus on the North Pacific area, since this region is dominated by interesting features such as: subduction zones at the rim of the oceanic Pacific plate and hot spots like the Hawaiian Island chain. A major advantage of this study is that it includes full-waveform modelling. In order to compare real waveform data to synthetics, usually a method to compute the latter is used. Our synthetic data was calculated using the spectral-element method, which is a numerical technique that solves the wave equation and allows us to obtain seismic recording using a more accurate numerical technique that takes into account the complex finite-frequency nature of the waves travelling through the Earth's interior (Tromp, 2015). Implementing the calculation of synthetic seismograms faces different challenges mostly because of the complex and heterogeneous structures inside the Earth. The synthetic data is calculated based on a 3D model (S40RTS) of the Earth. Instead of only looking at real data and create a model from there, we can find time sifts

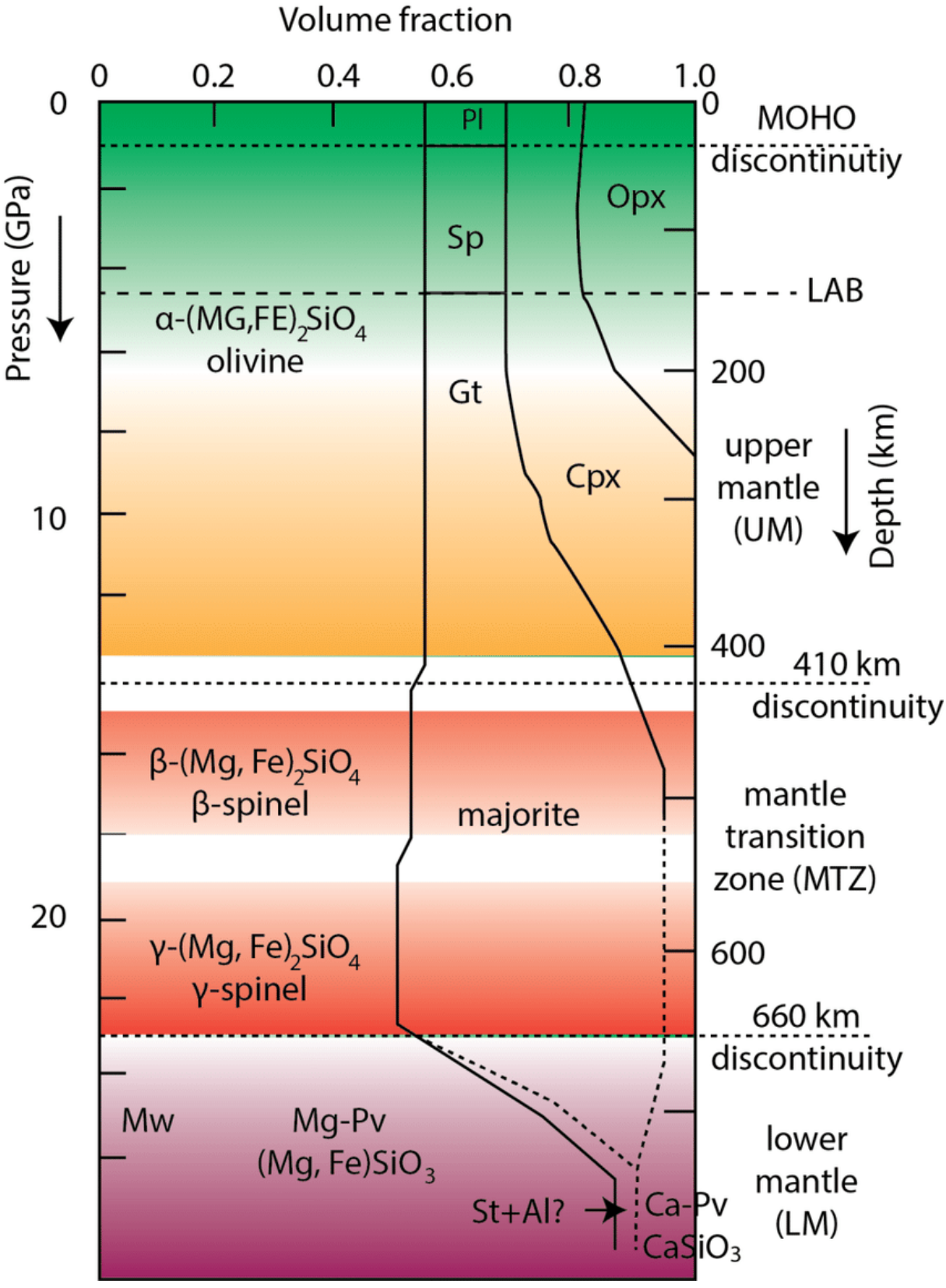

Figure 1: This is a simple illustration of Earth's mantle. Above the 410 km discontinuity α-olivine exists. The red color marks the transition zone between the discontinuities where wadsleyite exists. And the 660 km discontinuity marks the transition to the lower mantle colered in purple here. (Beniest, 2017)

by comparing a real seismogram to the corresponding synthetic seismogram and improve the existing model to a more precise model, given the information from the real data. The model used to compute the synthetic seismograms is a 3-D model of the Earth, which is based to the published model S40RTS (Ritsema, Deuss, van Heijst, & Woodhouse, 2011), and allows us to implement the topographic structure of discontinuities independently, for future use of the time shifts measured in this report.

There are many body wave seismic phases that have been frequently used to detect heterogeneities and discontinuities in the Earth's interior. The main goal of seismic imaging is to produce high resolution snapshots of the Earth's deep interior on different scales. Therefore, it is important to choose the right seismic phases, since they have different sensitivities depending on the structure and features one wants to image or investigate. Thus, in order to achieve high resolution we must consider all these different factors during data selection, which help us to optimise our imaging problem.

Considering the discontinuities bounding the transition zone in the mantle, namely at 410 km and 660 km depths, there is a great body of research, that includes studies with *PP* and *SS* precursor waves. These phases are used because they can provide a good global coverage in areas where it is usually difficult, such as the Pacific, because there are only few seismic stations. This is because precursor waves bounce off the discontinuity and they are very sensitive at the structure encountered beneath the bounce point at the aforementioned depths, respectively. The bounce point for SS and PP precursors is midway between the earthquake source and the receiver location as shown in Figure 2.

An important factor to be able to observe seismic phases of interest is the epicentral distance. It should be suitable for the chosen seismic phase. According to 1-D ray tracing, one can calculate the predicted traveltime arrival of phases of interest using TauP (Crotwell, Owens, & Ritsema, n.d.). This can help to choose the range of epicentral distances when the phases arrive rather isolated and make the right selection of stations, where measurements of time shifts between data and synthetics are more informative. In Figure 3, we plot travel time curves which shows the epicentral distance range and traveltime arrivals where each phase of interest in this report should be visible.

In this work, we focus on the SS precursors and ScS because these are waves which reflect off the major boundary interfaces in the mantle and are very sensitive to these structures. Starting with the SS precursors, a few well reported issues could be mentioned. These type of data are highly sensitive to discontinuity structure, however they can be very difficult to

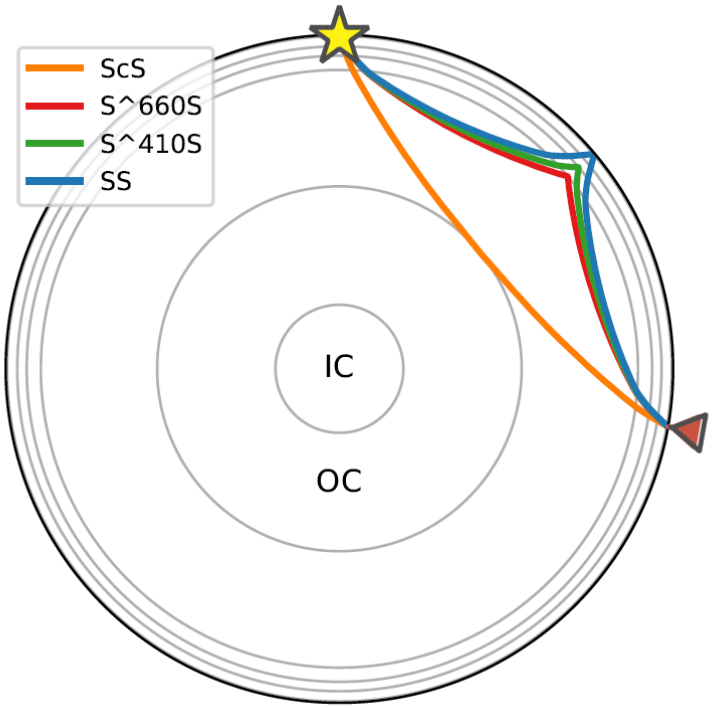

Figure 2: Theoretical raypaths of ScS, S410S, S660S and SS phase.

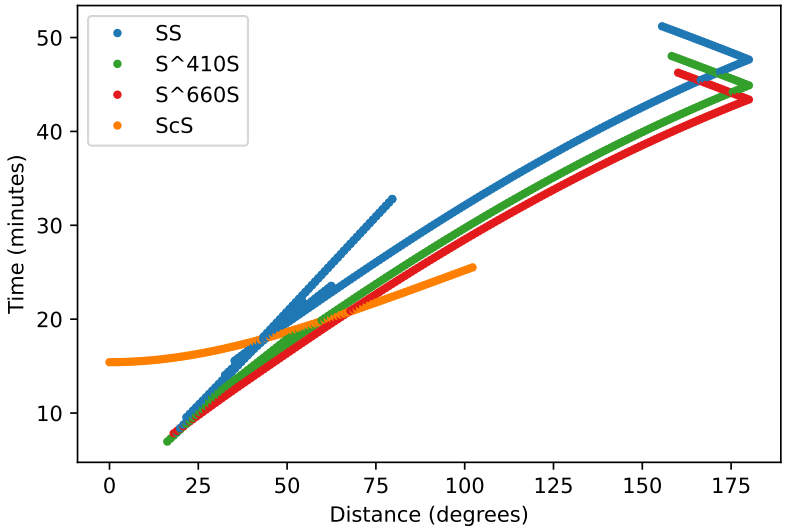

Figure 3: Travel time plot of different seismic S-phases. Plotted here are the ScS, S410S, S660S and the primary phase SS. The traveltime curves are calculated using the TauP method in obspy with PREM as a reference model. The ScS phase is only until 105° epicentral distance visible, while the other phases are visible until 180°.

observe in real waveforms. There can be loss of spatial resolution due to their relatively weak amplitude on real seismograms, which sometimes can barely be distinguished from noise. Due to this weak amplitude it is common to use stacking of coherent signals, e.g. (Zheng, Ventosa, & Romanowicz, 2015; Deuss, 2009). Precursor waves can also interfere with other seismic phases, such as the S_{diff} and the precursors of $ScSScS$ (Koroni, Bozdağ, Paulssen, & Trampert, 2017; Koroni, Paulssen, & Trampert, 2019), so it may be necessary to limit the epicentral distance range to make more robust observations. Usually we can see SS precursors within the range from 80-160° epicentral distances. The PP precursors have mainly the same characteristics as the SS precursors, but are more difficult to observe (Lessing, Thomas, Saki, Schmerr, & Vanacore, 2015a, 2015b). It has been suggested by researchers that the PP precursor data should be used within an epicentral distance of 80-140° (Deuss, 2009; Flanagan & Shearer, 1999), since they could interfere with the PKP phase beyond this range. It has been reported however that the 660 km discontinuity can only be detected in the SS precursor data, while it is absent in the PP precursor data (Deuss, 2009).

Besides the SS and PP precursor waves that are used in most studies (Zheng et al., 2015), the ScS phase and its reverberations is also used to detect discontinuities and reflectors. Revenaugh and Jordan (1991) used SH-polarized seismograms. There are vertically and horizontally polarized seismograms and P waves are better seen in vertical component seismograms and for S waves horizontal polarization is better (Deuss, 2009). The ScS phase is preferably used for more shallow discontinuities, that means above the 410 km discontinuity. With this phase the G-, X- and Lehmann Discontinuities have been found (Bagley & Revenaugh, 2008; Revenaugh & Jordan, 1991).

This study will show how to process and prepare real and synthetic data for further research. We explain the set up of the earthquake and the stations. The study of SS precursors allows us to get information on the topography of the discontinuities in the Earth's mantle. We apply a correlation function on a real and corresponding synthetic trace to evaluate the time shift. A linearised approach will give us the depth variation of the 410 km and 660 km discontinuity. Those variations are stored in a database (Table 1, 2 and 3). We will plot the resulting depth variation at the midlatitude and midlongitude bounce points and compare them to other studies.

3 Methods

3.1 Earthquake and data selection

The earthquake event from 28th April 2017 at 20:23 occurred near Mindanao, Philippines, at 5.49° latitude and 124.89° longitude and with Mw=6.9. Our real datasets are colletcted from Iris. For simplification we are using seismic data from only one earthquake with the purpose to set up the whole process and carefully assess the comparisons between real and synthetics at the time windows where the phases of interest is supposed to arrive. We chose an earthquake with a shallow focal depth of 31.35 km. Studies including precursor waves, most earthquakes have a depth around 30 km (Deuss, 2009). The magnitude is 6.9 which is consistent with earthquake magnitudes in other studies using precursors (Deuss, 2009), (Zheng et al., 2015), (Bagley & Revenaugh, 2008). We are using real data that is recorded by stations of the US array (Figure 4). We obtain waveforms from different stations all over the US mainland that we want to analyze. The epicentral distance of the stations ranges between 70°< Δ <140°. Zheng et al. (2015) chose an epicentral distance from 80°< Δ <160° and Deuss (2009) included in her precursor studies a station range from 100°< Δ <160°. The data is downloaded using the *mass_downloader* utility from Obspy. Our study includes the equivalent synthetic data, which will allow us to compare the real data and make a first approximation of the depth variation at the 410 km, 660 km discontinuities and core-mantle boundary, given the measured time shifts on the selected phases *ScS, S410S, S660S*.

3.2 Computing synthetic seismograms

The synthetic data are calculated using numerical wave propagation based on the spectral element method (Komatitsch & Tromp, 1999, 2002b, 2002a). The quality of a measurement between real data and synthetics can greatly depend on the resolution of the synthetic seismograms. Therefore, the spectral-element method allows us to make higher quality measurements, since it is capable of calculating the numerical solution of the wave equation in a more exact manner. There are several properties of seismic wave propagation, affecting the computation of synthetic seismograms, which have to be taken into account. For the synthetics calculated for the selected earthquake event, we use a mesh resolution which is equivalent to a dominant period of 11 seconds. Earth's properties as rotation, gravitation, attenuation and oceanic load are all taken into account (Tromp, 2015). This allows us to obtain seismograms as close as possible to realistic 3-D wave propagation through the Earth.

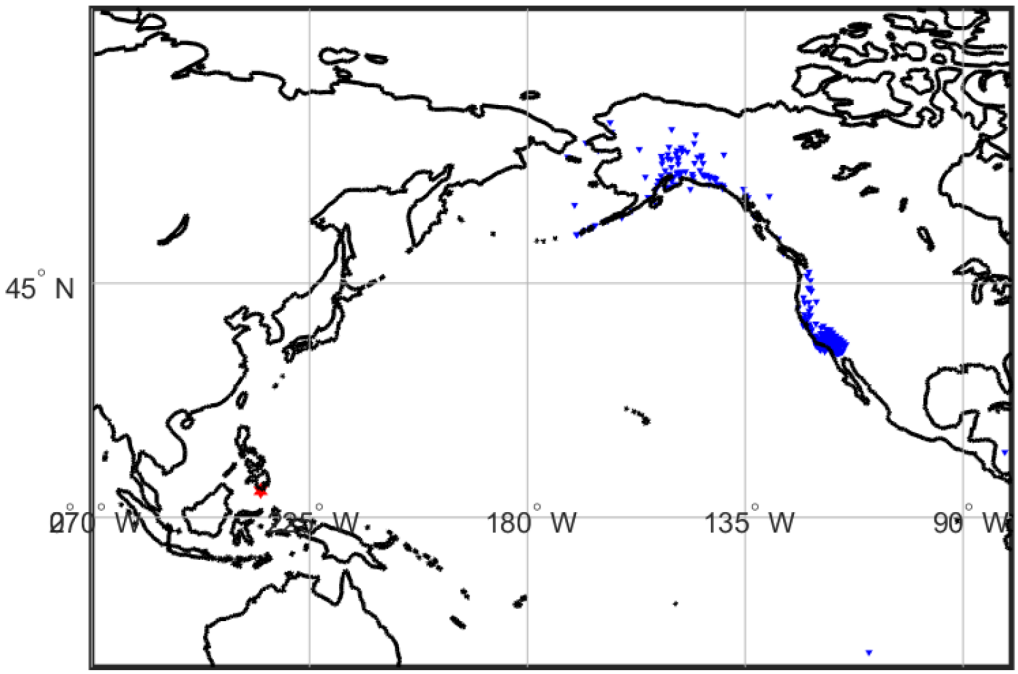

Figure 4: This map shows the region of research, i.e. the North Pacific Ocean. The earthquake is marked with a red star and the stations are marked with a blue, down-pointing triangle.

3.3 Data Processing

In Obspy we have different functions to prepare the data in order to analyze them. From the downloaded real data, the instrument response has to be removed, otherwise the seismograms can show significant amplitude and phase errors (Wilson, Ringler, Storm, Hutt, & Gee, 2013). These errors occur because the most commonly used seismograms do not measure the ground velocity directly, but a relative motion between the ground and a known inertial mass inside the seismograph. Python packages tailored for seismology, like Obspy, include functions that can de-convolve the instrument response (Lindsey, Rademacher, & Ajo-Franklin, 2020). While processing the data and later for the comparison of real and synthetic data, we need to pay attention to the sampling frequency. It has to be the same for all the traces of real and synthetic datasets. The sampling frequency has 6.2Hz, which means our sampling rate is 0.16s. Our data is filtered with a Butterworth bandpass filter with a frequency range from 0.01-0.08Hz. This bandpass is ideal for precursor studies as well as for the ScS seismic phase. It is also honouring the resolution of the synthetic seismograms and allows us to study these seismic phases. The synthetic data was processed in exactly the same way. We also normalized the data to treat the spurious amplitudes. We created separate vectors of the traces for each channel, named BHN, BHE and BHZ. The "rotate" function in Obspy converts the BHN and BHE components into a transverse and radial component.This allows us to have maximised SH wave energy to the transverse component, since we study phases which emanate and arrive at the stations as S-waves. Furthermore, we append the latitude and longitude attribute to each trace of the real data, so we can plot record sections. Within Obspy, we can calculate the epicentral distance of each station from the earthquake location and use this for further analysis and selection of appropriate trace recordings.

3.4 Plots of record sections

In order to see the desired SS precursors we analyze transverse polarized seismograms, since S phases have the highest energy content in the transverse component and therefore a higher amplitude in this polarisation direction. It makes them better visible. In the processing step we obtained a vector with traces only of the transverse component. We plotted a record section with all the travel time paths for the real and the synthetic data sets. This is an easy and clear way to see if we have a coherent signal of the SS precursors. A coherent signal indicates good data quality. In Figures 5, 6 a record section for the real and synthetic data is shown. The colored dots show the calculated arrival time of a phase of interest and an amplitude at the

same time shows the phase signal. In Figure 7 we can see how much the synthetic trace varies from each corresponding real trace.

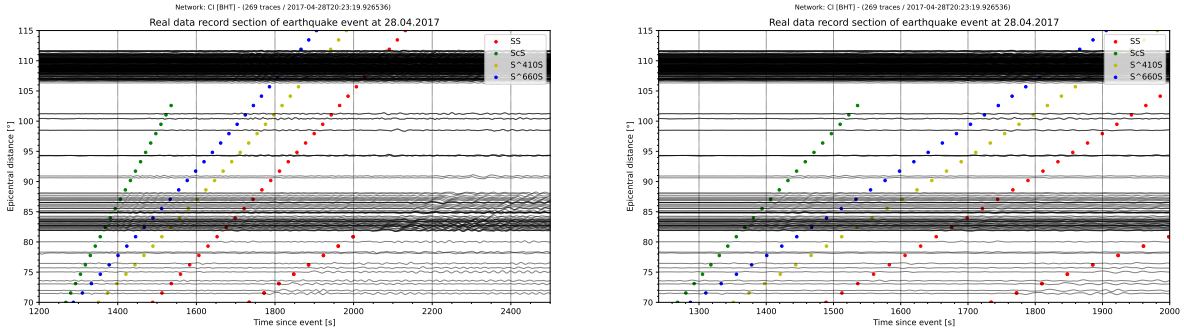

(a) The time axis is from 1200s to 2500s.

(b) Zoomed in time axis from 1240 to 2000s.

Figure 5: Record sections for the real data. The colored dots show the calculated arrival time at every distance according to PREM for each phase.

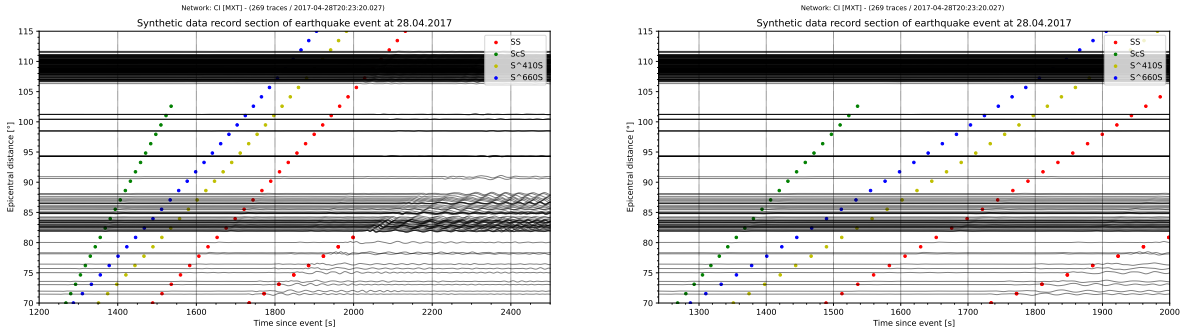

(a) The time axis is from 1200s to 2500s.

(b) Zoomed in time axis from 1240 to 2000s.

Figure 6: Record sections for the synthetic data. The colored dots show the calculated arrival time at every distance according to PREM for each phase.

3.5 Correlate real and synthetic data with regard to the ScS phase and the 410 km and 660 km SS precursor phase using narrow time windows

A common and efficient way to measure traveltime shifts when comparing real and synthetic seismograms is based on cross-correlation between the two signals. The purpose is to measure the time shift between a phase in the real data and the synthetic data. Therefore, we compare the real and synthetic seismograms one by one (Figure 8). We specifically search for SS precursors bouncing of at the 410 and 660 km discontinuity and the ScS phase reflecting off the core-mantle boundary. In order to find the phase of interest in the seismograms, 1D-ray-tracing is used to

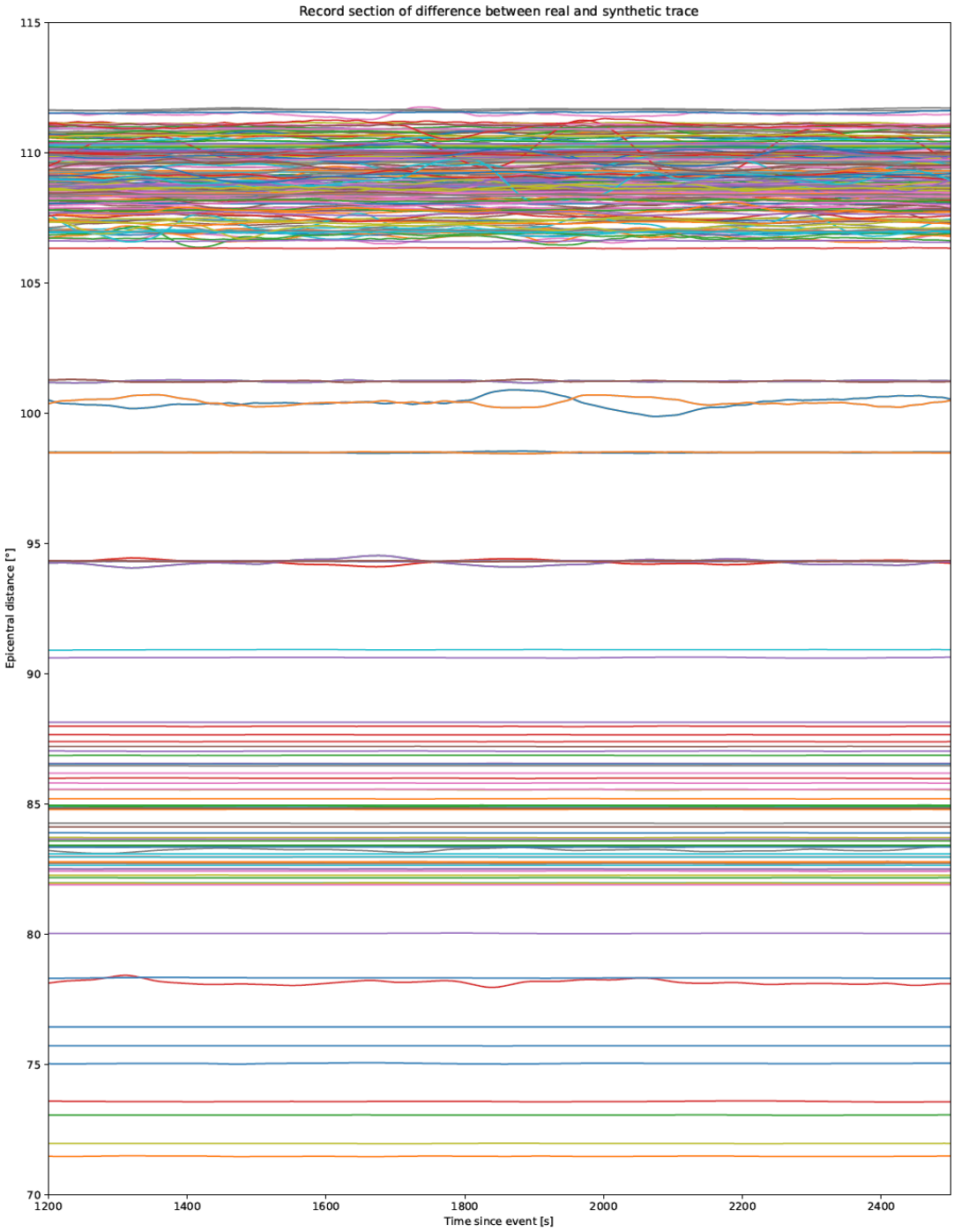

Figure 7: When we subtracted the synthetic trace from the real trace we received this differential trace. Here we see the differential record section plotted. The x axis just covers the body wave part of the seismogram from 1200 to 2500 seconds.

calculate a model based time at which the phase is supposed to arrive. For the calculation, we used the PREM model (Zheng et al., 2015) to be consistent with our selection of 3-D modelling, which is also based on the vertical velocity variations within the Earth as PREM. Obspy provides an implementation of the TauP toolkit, where the $get\_travel\_times() - Method$ gives the arrival time at a certain epicentral distance. It is desirable to compare the real and synthetic waveform only within the time window, a few seconds before and after the calculated arrival time of the phase of interest. Thus, we calculated the time window [-50,50] seconds, to make sure that the desired phase is within the cross-correlation time window.

At the highest point of the amplitude we can compute the time difference between observed and synthetic waveform using cross-correlation. Cross-correlation needs two time series and by multiplying the metric values at the same time step and summing all values, we get a correlation value. If the value is near 1 it means synthetic data and real data have a high correlation and a value near 0 indicates no correlation. The correlate()-function in Obspy needs three input parameters. First, we need two time series, in our case that would be a real trace and a synthetic trace. Secondly, we need a shift. With an empirical approach we set $shift = 100$. For each shift point and shifted in both directions it returns a correlation value, so we have 200 correlation values. Since we are only interested in the highest value, Obspy provides a function $xcorr\_max()$. This function gives back two values: the shift value and the corresponding highest correlation value. We chose to select the traces with a correlation coefficient value higher than 0.5 and calculate the time shift for further use. The actual time shift is the shift value we obtained from the $xcorr\_max() - function$ multiplied by the sampling rate. The sampling rate is $\frac{1}{6.2Hz} = 0.16s$. This led to less traces participating in the data set, but with a better quality within the time windows around S410S, S660S and ScS.

3.6 Linearised inference of variation of discontinuity reference depths using ray theory

The obtained time shifts are used as a first approach to get an impression of the variation of discontinuity depths at the locations where the ray paths interact with the respective discontinuity. These are the midpoints between source and receiver. We are using a linearised approach for obtaining the depth variation in terms of the time shift, explained in the following passage.

There is a simple expression that we can use to relate the calculated travel time difference δt^{rt} to the depth δh, which denotes a variation of the reference discontinuity depth. This expression

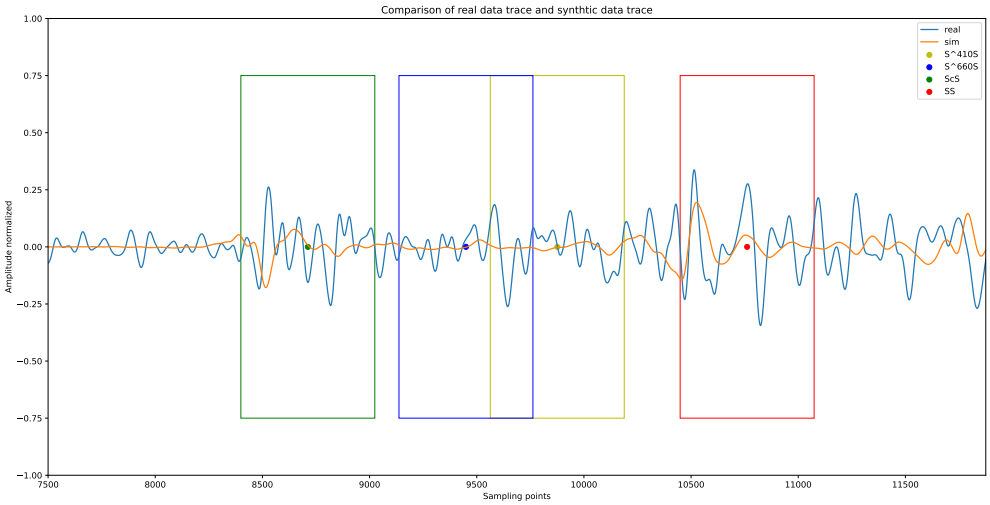
Comparison of real data trace and synthtic data trace
real
sim
S^410S
S^660S
ScS
SS
Amplitude normalized
Sampling points

(a)

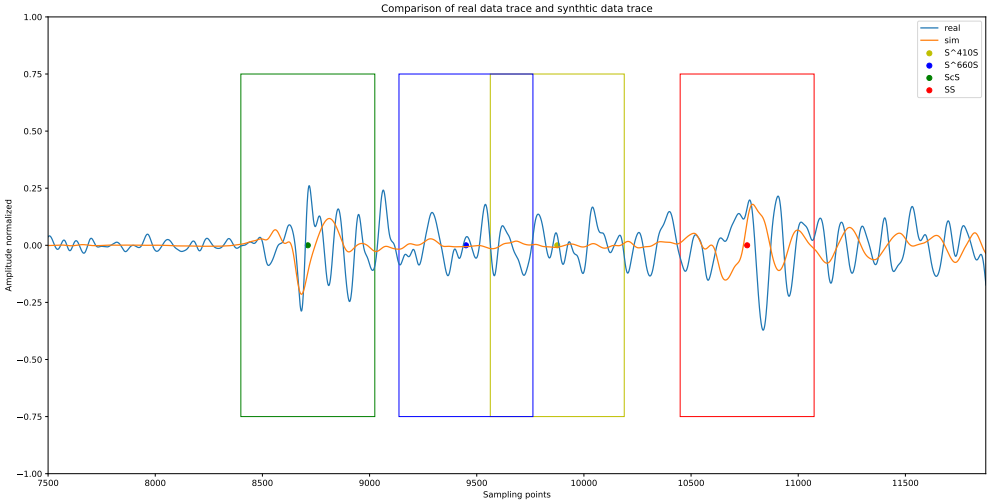
Comparison of real data trace and synthtic data trace
real
sim
S^410S
S^660S
ScS
SS
Amplitude normalized
Sampling points

(b)

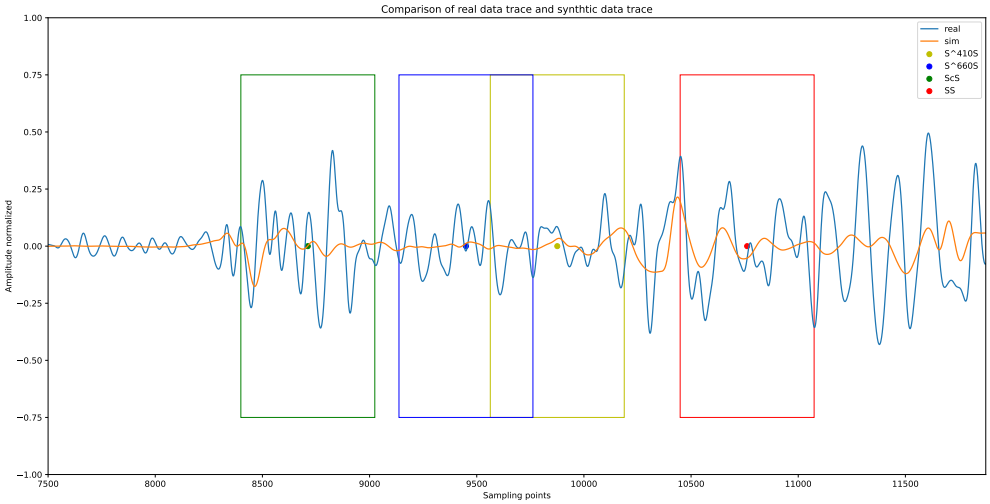

(c)

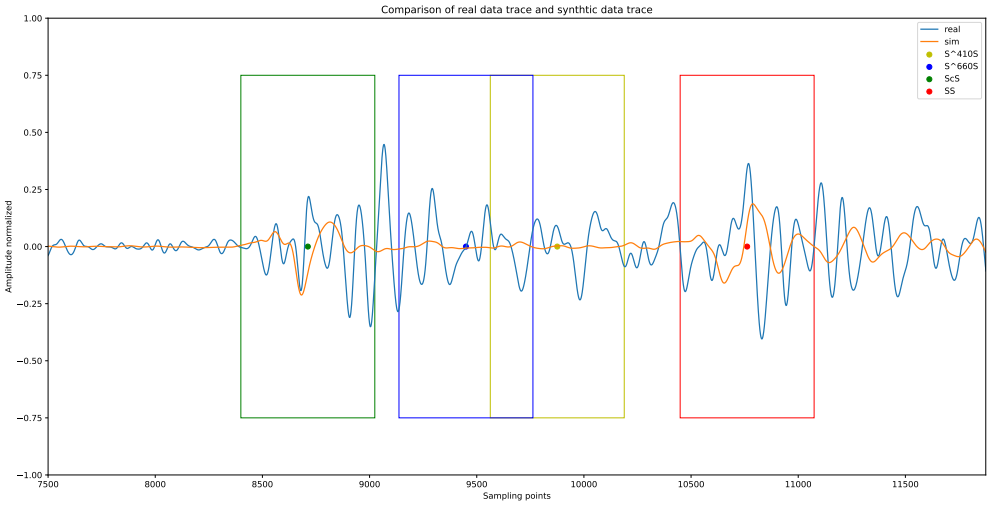

(d)

Figure 8: Here we have a one by one comparison of a real and synthetic trace. The x-axis shows the data points and between two data points are 0.16s. The colored dots show the calculated arrival time and we have a corresponding time window of +-50s around each point. The traces are only correlated inside these windows. (a)-(d) show different correlated traces.

can be written as follows for the 410 km, 660 km discontinuity and CMB:

$$\delta t^{rt} = \frac{-2\delta h \cos i}{v_s}$$

, i is the reflection angle of the wave at the bounce point and v_s is the S-wave velocity. For the two mantle discontinuities i is set to 20° and V_s for the 410 km discontinuity is 4.93 km/s and for the 660 km discontinuity 5.94 km/s. For the angle i at the CMB we need a steeper value of 60° and a velocity of 7.2 km/s. With the measured travel time difference we can correct the discontinuity depth by δh.

We made three databases for the ScS phase, the S410S and S660S precursors. In the databases, the travel time shifts and the corresponding calculated depth variation are stored together with the name of the station and the geographical coordinates. They are appended at the end of the report.

Our databases (Tables 1, 2 and 3) only have traces from one single earthquake event and therefore the area is not very well sampled. If we want to get to know the structure beneath the Earth's surface better and acquire an understanding for the dynamical processes of the mantle we need a much better data coverage. An easy way in our study to increase the sampling coverage would be more synthetic traces calculated for corresponding real traces. Most other studies use more than one earthquake source, in order to have waves travelling the entire mantle. In that case we would not just have one event with a latitude and longitude and one origin time, but a list with different latitudes and longitudes and origin times. In the jupyter notebook we looped waveform and station list to find the matching ones and for multiple earthquakes we loop the list with all the event parameters and match the traces to the earthquake.

4 Results & Discussion

The travel time shift databases allow us to plot maps with the discontinuity depth showing a deviation from the reference depth in PREM (410 km or 660 km). In the appendix, we present the tables for each phase with columns of the absolute discontinuity depth as well as the latitude and longitude of the bounce point corresponding to each trace. In Figures 10, 11 and 12, the absolute discontinuity depth at a certain latitude and longitude is shown. The color bar has a kilometer scale.

Our data is not very evenly distributed and we only have few data points after removing not well correlated data and synthetics and since we use one earthquake event. They are located before the east coast of Japan and in the middle of the North Pacific around 175° longitude and

35° latitude. We explain the resulting topography of upper mantle discontinuities considering the expectation of uplift or depression given the geological vicinity and the thermal factors that can introduce topography. The Clapeyron slope for the phase transition to wadsleyite at 410 km depth is positive (Houser & Williams, 2010). So the phase transition moves to higher pressures (i.e. greater depths) under warm anomalies and to lower pressures (i.e. shallower depths) under cold anomalies. At 660 km depth we have the phase transformation to perskovite and magnesiowüstite that goes with a negative Clapeyron slope. This is the reason why the 660 km discontinuity reacts exactly opposite to the 410 km discontinuity. Under warm anomalies it should be shallower and beneath cold anomalies deepened.

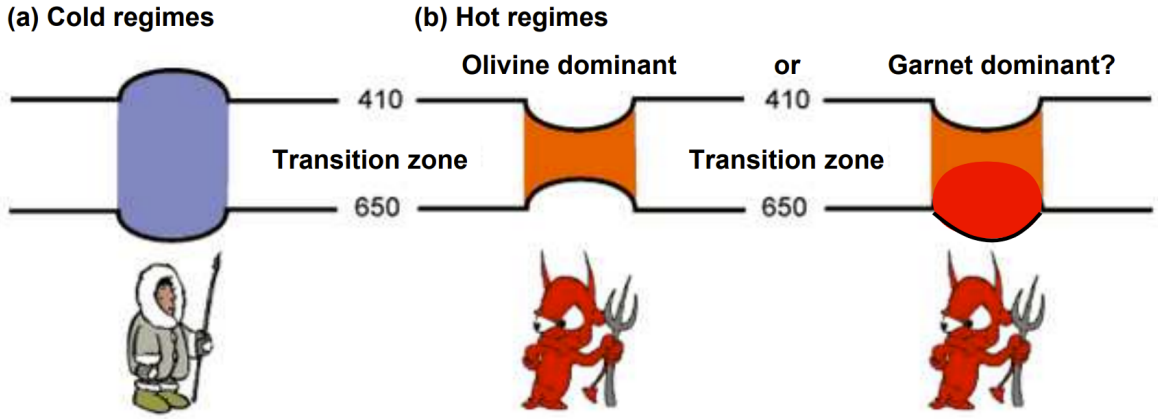

Figure 9: Illustration of how the discontinuities behave under cold and warm anomalies according to the Clapeyron slope

(Deuss, 2007)

4.1 The 410 km Discontinuity

In our preferred 1-D model PREM, the 410 km discontinuity is prominently seen and is characterised by a velocity increase. In the work of Deuss (2009) a globally consistent signal of the SS precursors is observed by stacking them. Stacking is a processing step that allows us to see if the traces have a signal from the phase of interest and to make them more visible, since the precursors are often at or below noise level.

It is common to measure directly the topography of the discontinuities, however, a more robust measurement can be the thickness of the transition zone, as it is performed by Deuss (2009). The robustness comes from the fact that the transition zone thickness does not depend on mantle and crustal corrections above the transition zone(Deuss, 2009). The thickness of the

transition zone is the difference between the topography of the 410 km and 660 km discontinuity. In the aforementioned work, it is found that a thickened transition zone occurs beneath regions of subduction zones (Deuss, 2009). Zheng et al. (2015) studied part of the region in the Pacific and found a slightly shallower 410 km discontinuity at the Northwest rim of the Pacific. They had as well data in the Hawaiian island chain region and the tomography plot showed depth variations of about +10 km in this region. Like Deuss they measured as well the transition zone thickness and there is more clearly seen that it is thickened beneath the subduction zone in the northwest Pacific. We can see a nicely thinned transition zone around Hawaii, corresponding to higher than average mantle temperatures, owing to the ascending hot material from the lower mantle. However, studies do not always agree, for example in his extended work, Shearer (2000) found in his paper a deepening of the 410 km discontinuity.

Amongst the vast amount of publications concerned with studying the mantle discontinuities, there are still significant differences about the depth of the discontinuities. It is possible that they are due to differences in the processing steps or the mantle and crustal corrections above the discontinuity (Bai, Zhang, & Ritsema, 2012; Koroni & Trampert, 2016). We have to stress the fact that for our study, we did not perform stacking of the traces to make sure that there actually is a coherent signal and we left out the upper mantle and crustal corrections when doing the calculations for the depths. Future work on imaging upper-mantle discontinuities would require and greatly benefit from these additional correction steps and collection of more earthquake data.

As we can extract from Table 1 our depth variations of the 410 km discontinuity ranges between about +-50 km. Figure 10 shows 130 points with the depth variation, which are not very evenly distributed. We have data close to the East coast of Japan. Most of the depths there are around 400 km depth, which would indicate a shallower depth and be consistent with studies of Deuss, Zheng et al. or Houser and Williams. We have an average depth for the 410 km discontinuity of 405 km from our data, which is slightly bigger than the global averaged depth in PREM. Since we have only data points in the Northwestern part of the Pacific, which is close to a subduction zone, the data matches our expectation, given colder regimes, and show some similarities with the other studies.

4.2 The 660 km Discontinuity

The 660 km discontinuity should behave exactly opposite to the 410 km discontinuity if, as we assume, the variations of the topography are due to thermal anomalies. Zheng et al. (2015)

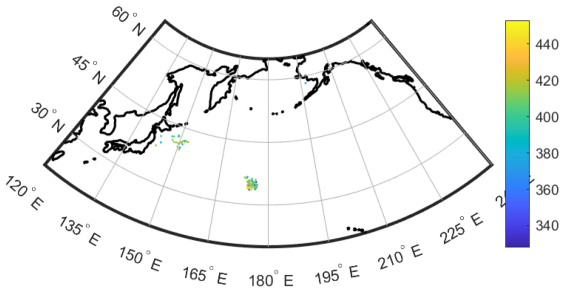

(a) Map with all 130 data points near the East coast of Japan.

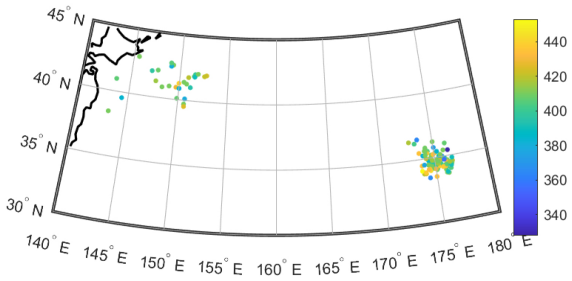

(b) Zoomed in map.

Figure 10: Colored dots show the depth displacement of the 410 km discontinuity at the latitude and longitude of the bounce points from each trace.

found the deepest discontinuity depth, at around 680 km, right under the Northwestern rim of the Pacific Ocean and under the warm anomaly like the Hawaiian hot spot the depth is shallower than 660 km. Houser and Williams (2010) reported as well a deepened 660 km discontinuity. Shearer (2000) also made extensive research on the 410 km and 660 km discontinuities. He found a correlation of a depressed 660 km discontinuity topography and subduction zones.

The mean value for the data points of the 660 km discontinuity lies at 658 km. Thus, we do not seem to have a significant change in the depth of the discontinuity overall. In Table 2 we calculated a discontinuity depth variation mostly from +-40 km. There are three values that show depth variations for about -90 km and +70 km. The value is in good agreement with the Pacific average value of 658 km from Schmerr, Garnero, and McNamara (2010) and Zheng et al. (2015), who reported an average value of 648 km from their data in the Pacific ocean. But nevertheless our average value is against our expectations, since our data points are located near the Northwestern subduction zone of the North Pacific. If anything we expect a slight deepening of the 660 km discontinuity. It is also a simplifying assumption that the topography variations are only due to the thermal anomalies. Shearer (2000) postulates that the two discontinuities are largely uncorrelated.

4.3 Core-mantle boundary

The study of the core-mantle boundary is still a subject of today's research, since we have poorly consistent results on the topography of the CMB (Souriau, 2007). Above the CMB we have a 150-300 km thick layer, called the D" layer. It is characterized by significant lateral heterogeneity, a much lower velocity gradient and in some regions the velocity decreases considerably (Revenough,

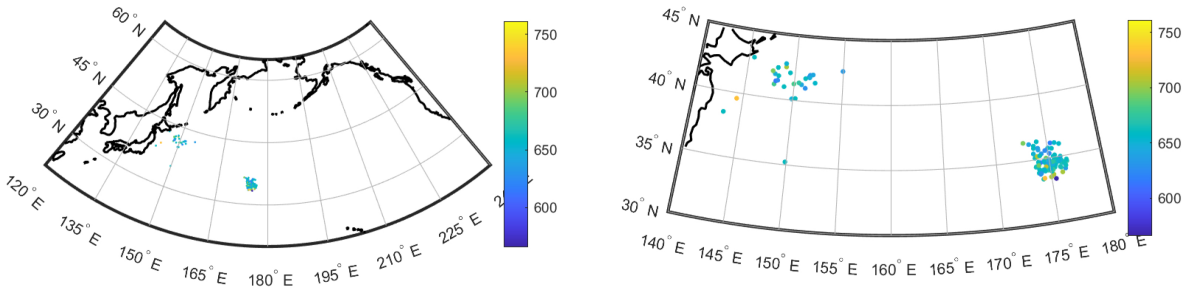

(a) Map with all 129 data points near the East coast of Japan.

(b) Zoomed in map.

Figure 11: Colored dots show the depth displacement of the 660 km discontinuity at the latitude and longitude of the bounce points from each trace.

1991). It is interesting to study the CMB below the Pacific, because it is one of two large low shear-wave velocity provinces. They have an extension of a few thousand kilometers and the velocity in the mantle of this region drops a few percent (Koroni et al., 2021, submitted).

For studies of the core-mantle boundary PcP, PKP or PKKP phases can be used in rather high frequencies. Latter phase would be preferable because it only samples the topography of the CMB, but unfortunately it is very difficult to observe (Souriau, 2007). Core-mantle boundary reflected S-phases could also provide an option, as they directly interact with the CMB. In the data received from the other phases there always seems to be a contamination from the D" layer, and since it is poorly known, the trade off between boundary topography and velocity structure just above can hinder the possibility of obtaining a good quality CMB topography model. (Revenaugh & Jordan, 1991c) use the ScS phase to do research on the core mantle boundary.

Similarly, in our study we used the ScS phase to calculate the time shift and therefore translate it to the depth variation at the CMB. We were able to extract only 37 depth variation data points, after quality measurements. That is over four times less than for the selected precursor data, regarding the 410 km and 660 km discontinuities. So we can see that it is already difficult to achieve the same amount of information, but nonetheless we have acquired a database that can be analysed or further expanded, in a larger study with more earthquakes. The depth in our study varies in a range of tens of kilometers. This seems to agree with the range that Souriau (2007) mentioned. However, there is no clear agreement on which seismic phases can provide more robust constraints of the CMB topography. Therefore, we expect that the results shown here are merely an indication of the ScS phase potential for further studying

the CMB topography.

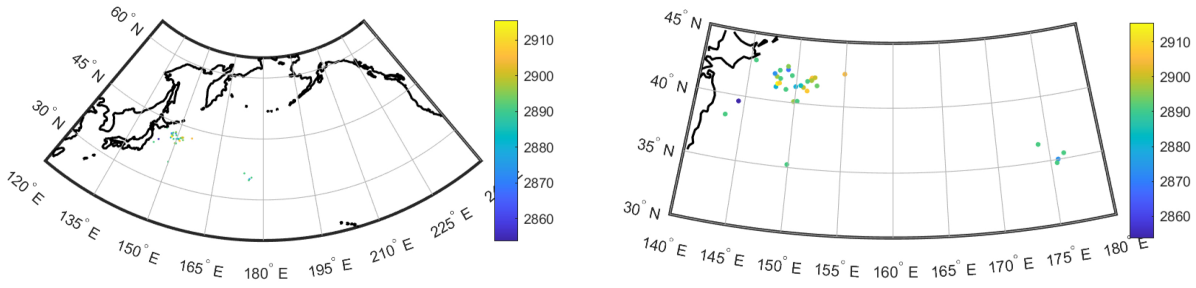

(a) Map with all 37 data points near the East coast of Japan.

(b) Zoomed in map.

Figure 12: Colored dots show the depth displacement of the CMB at the latitude and longitude of the bounce points from each trace.

5 Conclusion

The goal of this study was to further develop a code to process real seismic data, so they can be used for further research. We used Obspy to do all the processing steps. It is important to remove the instrument response from the data and to make sure that the sampling rate is the same in every trace, so we can compare them. The data is filtered using a Butterworth-bandpass with corners from 12.5-100 s. In order for us to get high resolution tomography models from the Earth's mantle, we used synthetic data calculated with the spectral element method. This full-waveform modelling approach solves the wave equation very accurately and therefore we have high resolution synthetic data. We made a jupyter-notebook for processing the real and synthetic data and all the calculations for the discontinuity depths. The notebook can be easily adapted for more earthquakes.

We wanted to make depth measurements for the topography of the mantle discontinuities. One by one comparison using the maximum of the cross-correlation between real and synthetic seismograms gives us the travel time difference between them. With a linearised approach we calculated the depth variation of the discontinuities and stored them in databases.

We assumed that the depth variation is mostly due to thermal anomalies and behave according the Clapeyron slope. That suggests under cold anomalies a shallower 410 km discontinuity and a deepened 660 km discontinuity are expected, and vise versa for warm anomalies. The depth variation of the 410 km and 660 km discontinuity show some similarities with the papers

we compared, like Deuss, Zheng et al. and Shearer. The mean depth of the 410 km discontinuity in the North West Pacific is found on average at 405 km. That is consistent with our expectations of a shallower 410 km discontinuity. We did not see as clear results for the 660 km discontinuity. The mean value was not significantly lower with 658 km, but we expected a deeper 660 km discontinuity due the Clapeyron slope.

Nonetheless, there are still some significant differences between various papers that mapped the discontinuity depths. The SS precursor and ScS data is sensitive to upper mantle and crustal corrections that have to be made for the discontinuity depth or the fact that the variations in topography are also due to chemical heterogeneities and not only thermal anomalies. For exemplifying reasons, we analyzed only one earthquake and had therefore a low sampling density. We did not perform stacking or the above mentioned corrections as it usually done in other studies.

A Databases for the 660 km and 410 km discontinuity and CMB

Table 1: Data of the 410 km discontinuity

	traces410	latitude410	longitude410	distance410	timeshift410	deltadepth410	absdepth410	mlatitude410	mlongitude410
0	AK.ANM..BHT	64.5646	-165.3732	76.4399725213	4.36050010084	-26.3393904177	383.660609582	39.5691	144.3745
1	AK.BAL..BHT	61.035999	-142.346207	86.5336374226	0.32300000747	-1.95106595687	408.048934043	41.8986	151.4643
2	AK.BARN..BHT	61.059502	-141.662201	86.8610931818	1.61500003735	-9.75532978435	400.244670216	42.0483	151.5694
3	AK.BCP..BHT	59.9534	-139.6369	87.9782907902	-2.09950004855	12.6819287197	422.68192872	42.0189	152.756
4	AK.BRSE..BHT	59.741699	-150.741394	82.4230391751	0.0	-0.0	410.0	39.7127	150.6339
5	AK.CAPN..BHT	60.768299	-151.1539	82.2604431686	0.484500011205	-2.9265989353	407.073401065	40.0974	149.8823
6	AK.CHUM..BHT	63.882702	-152.315201	81.9022265672	-0.807500018675	4.87766489217	414.877664892	41.2368	147.5656
7	AK.CNP..BHT	59.5251	-151.2373	82.1638869333	-2.42250005602	14.6329946765	424.632994677	39.524	150.6573
8	AK.COLD..BHT	67.226898	-150.203796	82.9679829755	0.0	-0.0	410.0	42.9068	145.5194
9	AK.CUT..BHT	62.4058	-150.262497	82.7500750785	0.0	-0.0	410.0	40.9677	148.9798
10	AK.DIV..BHT	61.1292	-145.7749	84.8733053266	0.0	-0.0	410.0	41.2568	150.7526
11	AK.DOT..BHT	63.648201	-144.069702	85.5431473684	0.0	-0.0	410.0	42.6073	149.2093
12	AK.EYAK..BHT	60.548698	-145.75	84.9068305417	2.58400005976	-15.608527655	394.391472345	41.0139	151.1646
13	AK.GAMB..BHT	63.775799	-171.703598	73.5767286149	0.0	-0.0	410.0	38.399	143.2888
14	AK.GHO..BHT	61.771	-148.925995	83.3601581482	-3.06850007096	18.5351265903	428.53512659	40.9374	149.6821
15	AK.GLB..BHT	61.4417	-143.8123	85.7990449376	-1.61500003735	9.75532978435	419.755329784	41.7718	150.8996
16	AK.KIAG..BHT	60.9231	-142.360504	86.5367132547	3.39150007843	-20.4861925471	389.513807453	41.8491	151.5449
17	AK.KLU..BHT	61.4924	-145.9227	84.7897530282	0.0	-0.0	410.0	41.3816	150.467
18	AK.KNK..BHT	61.413101	-148.458496	83.57924736	4.52200010458	-27.3149233962	382.685076604	40.8701	150.0215
19	AK.KOTZ..BHT	66.895103	-162.600006	78.1474711329	0.64600001494	-3.90213191374	406.097868086	40.9572	143.5585
20	AK.LOGN..BHT	60.824001	-141.004807	87.2031300645	0.0	-0.0	410.0	42.0878	151.8616
21	AK.MLY..BHT	65.030403	-150.744202	82.6469010861	2.26100005229	-13.6574616981	396.342538302	41.9683	147.0511
22	AK.NEA2..BHT	64.5928	-149.0694	83.3439719311	0.32300000747	-1.95106595687	408.048934043	42.0775	147.6617
23	AK.PIN..BHT	60.095901	-140.252502	87.6552664284	-1.77650004108	10.7308627628	420.730862763	41.946	152.5391
24	AK.PPLA..BHT	62.896198	-152.189407	81.8908796046	0.0	-0.0	410.0	40.8418	148.2598
25	AK.RIDG..BHT	63.7399	-144.8462	85.1946773227	4.68350010831	-28.2904563746	381.709543625	42.4976	149.0124

26	AK.SCM..BHT	61.832001	-147.328995	84.1148253765	-4.84500011205	29.265989353	439.265989353	41.2583	149.9557
27	AK.SCRK..BHT	63.976101	-143.990494	85.5586185659	0.807500018675	-4.87766489217	405.122335108	42.749	148.9713
28	AK.SWD..BHT	60.1043	-149.4526	83.0785293059	5.16800011952	-31.2170553099	378.78294469	40.1132	150.6876
29	CI.BBR..BHT	34.2623	-116.92075	109.557903904	0.0	-0.0	410.0	34.85	175.2749
30	CI.BBS..BHT	33.92139	-116.98058	109.635703096	2.26100005229	-13.6574616981	396.342538302	34.5895	175.44
31	CI.BEL..BHT	34.0006	-115.9982	94.2780024179	6.9445001606	-41.9479180727	368.052081927	35.0211	175.7222
32	CI.BEL..BHT	34.0006	-115.9982	94.2780024179	6.9445001606	-41.9479180727	368.052081927	35.0211	175.7222
33	CI.BLA2..BHT	34.06931	-116.38993	110.037295879	-2.58400005976	15.608527655	425.608527655	34.9181	175.5556
34	CI.BLC..BHT	34.24356	-118.67312	108.210652217	-2.90700006723	17.5595936118	427.559593612	34.1857	174.699
35	CI.BLY..BHT	33.7503	-114.52375	98.4909078357	13.5660003137	-81.9447701885	328.055229811	35.4261	176.3422
36	CI.BLY..BHT	33.7503	-114.52375	98.4909078357	13.5660003137	-81.9447701885	328.055229811	35.4261	176.3422
37	CI.BOM..BHT	33.36465	-115.72963	110.808854111	0.0	-0.0	410.0	34.6768	176.1586
38	CI.BOR..BHT	33.2682	-116.41716	110.310396454	0.0	-0.0	410.0	34.3434	175.9795
39	CI.BRE..BHT	33.80776	-117.98116	108.900035425	4.03750009337	-24.3883244609	385.611675539	34.1361	175.1636
40	CI.BTP..BHT	34.68224	-118.57398	108.13489248	-3.06850007096	18.5351265903	428.53512659	34.5245	174.4987
41	CI.CAR..BHT	35.30819	-119.84583	106.941340517	-4.03750009337	24.3883244609	434.388324461	34.4925	173.7389
42	CI.CCC..BHT	35.52495	-117.36453	108.757314264	0.807500018675	-4.87766489217	405.122335108	35.5495	174.4294
43	CI.CHF..BHT	34.333408	-118.025848	108.680307201	2.26100005229	-13.6574616981	396.342538302	34.4854	174.869
44	CI.CJM..BHT	34.27117	-117.42448	109.166652029	-1.29200002988	7.80426382748	417.804263827	34.6662	175.1031
45	CI.CLC..BHT	35.81574	-117.59751	108.474737096	0.484500011205	-2.9265989353	407.073401065	35.6585	174.1905
46	CI.CLT..BHT	34.09284	-117.31687	109.313835193	1.13050002614	-6.82873084904	403.171269151	34.5825	175.2353
47	CI.COA..BHT	32.86341	-115.12339	111.467429834	-1.61500003735	9.75532978435	419.755329784	34.5561	176.6325
48	CI.CTW..BHT	33.67728	-115.87214	110.582031276	4.84500011205	-29.265989353	380.734010647	34.8426	175.9411
49	CI.DEV..BHT	33.93597	-116.57794	94.3169834731	5.65250013072	-34.1436542452	375.856345755	34.7528	175.5662
50	CI.DEV..BHT	33.93597	-116.57794	94.3169834731	5.65250013072	-34.1436542452	375.856345755	34.7528	175.5662
51	CI.DJJ..BHT	34.10618	-118.45505	108.427500352	0.0	-0.0	410.0	34.17	174.8454
52	CI.DPP..BHT	32.99889	-116.94187	109.997978039	0.0	-0.0	410.0	33.953	175.943
53	CI.DRE..BHT	32.80532	-115.44679	100.413574054	0.0	-0.0	410.0	34.3877	176.5546
54	CI.DRE..BHT	32.80532	-115.44679	100.413574054	0.0	-0.0	410.0	34.3877	176.5546

55	CI.DSC..BHT	35.14255	-116.10395	109.854111446	6.29850014566	-38.045786159	371.954213841	35.7715	175.0474
56	CI.EDW2..BHT	34.8811	-117.99388	108.510582143	-0.32300000747	1.95106595687	411.951065957	34.8747	174.5831
57	CI.FOX2..BHT	34.7339	-118.24046	108.373489461	1.45350003361	-8.77979680591	401.220203194	34.6825	174.5818
58	CI.FUR..BHT	48.1639	11.2768	101.22532215	4.84500011205	-29.265989353	380.734010647	41.5581	84.744
59	CI.FUR..BHT	48.1639	11.2768	101.22532215	4.84500011205	-29.265989353	380.734010647	41.5581	84.744
60	CI.GLA..BHT	33.05149	-114.82706	111.626357352	3.39150007843	-20.4861925471	389.513807453	34.8079	176.6296
61	CI.GMA..BHT	34.29148	-116.38256	109.960706192	3.2300000747	-19.5106595687	390.489340431	35.0759	175.4357
62	CI.GR2..BHT	34.11816	-118.30024	108.543475935	3.7145000859	-22.437258504	387.562741496	34.235	174.8914
63	CI.GRA..BHT	36.99608	-117.36621	108.211268344	7.59050017554	-45.8500499864	364.149950014	36.5328	173.5779
64	CI.HAR..BHT	35.0114	-117.29909	108.994817571	0.0	-0.0	410.0	35.2241	174.7382
65	CI.HMT2..BHT	33.708115	-117.001524	109.696614244	1.13050002614	-6.82873084904	403.171269151	34.432	175.5476
66	CI.HOL..BHT	34.45831	-117.84539	108.775260019	2.09950004855	-12.6819287197	397.31807128	34.6387	174.862
67	CI.IDO..BHT	33.79678	-116.22152	110.267887877	0.0	-0.0	410.0	34.7918	175.7602
68	CI.IKP..BHT	32.65012	-116.10948	110.776211791	0.807500018675	-4.87766489217	405.122335108	34.02	176.4111
69	CI.IRM..BHT	34.15738	-115.14513	110.958833684	-0.161500003735	0.975532978435	410.975532978	35.4649	175.9125
70	CI.JEM..BHT	33.08098	-116.59755	110.237754008	1.93800004482	-11.7063957412	398.293604259	34.1417	176.0176
71	CI.LCP..BHT	34.73551	-120.27996	106.797930529	2.74550006349	-16.5840606334	393.415939367	33.9493	173.8953
72	CI.LDR..BHT	34.9906	-118.34156	108.205249093	4.03750009337	-24.3883244609	385.611675539	34.8212	174.4089
73	CI.LGB..BHT	33.9753	-118.14918	108.710687078	2.58400005976	-15.608527655	394.391472345	34.1912	175.0181
74	CI.LJR..BHT	34.80762	-118.86775	107.864966284	0.0	-0.0	410.0	34.5034	174.3334
75	CI.LMR2..BHT	34.93439	-117.69629	108.719353647	0.0	-0.0	410.0	35.0221	174.6515
76	CI.LOC..BHT	34.690735	-120.446901	106.683158005	-1.61500003735	9.75532978435	419.755329784	33.8602	173.8616
77	CI.LRL..BHT	35.47954	-117.68212	108.533139251	-4.36050010084	26.3393904177	436.339390418	35.3993	174.3532
78	CI.LUG..BHT	34.3656	-117.36683	109.177081364	0.0	-0.0	410.0	34.7534	175.0711
79	CI.MCT..BHT	34.22645	-116.04073	110.247116895	0.0	-0.0	410.0	35.1625	175.5834
80	CI.MLAC..BHT	37.63019	-118.83605	106.891096755	-1.29200002988	7.80426382748	417.804263827	36.3992	172.7571
81	CI.MLS..BHT	42.9578	1.0947	109.877750086	-1.93800004482	11.7063957412	421.706395741	42.6239	78.7906
82	CI.MLS..BHT	42.9578	1.0947	109.877750086	-1.93800004482	11.7063957412	421.706395741	42.6239	78.7906
83	CI.MTG..BHT	33.19915	-116.64727	110.156175829	-3.87600008964	23.4127914824	433.412791482	34.2068	175.9382

84	CI.MTP..BHT	35.48434	-115.5532	154.260780981	0.0	-0.0	410.0	36.2204	175.0227
85	CI.MTP..BHT	35.48434	-115.5532	154.260780981	0.0	-0.0	410.0	36.2204	175.0227
86	CI.NBS..BHT	34.78035	-116.55798	109.645038031	-3.55300008217	21.4617255256	431.461725526	35.3473	175.1069
87	CI.NJQ..BHT	34.53412	-120.17737	106.944241155	-2.09950004855	12.6819287197	422.68192872	33.8476	174.0351
88	CI.NSS2..BHT	33.55553	-115.94586	110.57037864	0.0	-0.0	410.0	34.7281	175.983
89	CI.OLP..BHT	32.60771	-116.93019	110.146682844	0.0	-0.0	410.0	33.6781	176.1502
90	CI.PALA..BHT	33.38905	-117.03182	109.78790251	-4.52200010458	27.3149233962	437.314923396	34.1958	175.7071
91	CI.PASC.00.BHT	34.17141	-118.18523	108.614010636	-0.484500011205	2.9265989353	412.926598935	34.3143	174.902
92	CI.PDE..BHT	34.44199	-118.58215	108.212292797	0.0	-0.0	410.0	34.356	174.6244
93	CI.PDM..BHT	34.30336	-114.14152	111.666123279	0.484500011205	-2.9265989353	407.073401065	35.9692	176.1495
94	CI.PLS..BHT	33.7953	-117.60906	109.19373851	-4.52200010458	27.3149233962	437.314923396	34.2654	175.2963
95	CI.PSR..BHT	34.09181	-117.80709	108.93498382	2.26100005229	-13.6574616981	396.342538302	34.3987	175.0717
96	CI.RAG..BHT	34.68289	-116.15139	109.991401699	4.19900009711	-25.3638574393	384.636142561	35.4367	175.2927
97	CI.RRX..BHT	34.87533	-116.99684	109.275187121	-4.19900009711	25.3638574393	435.363857439	35.2451	174.9119
98	CI.RVR..BHT	33.99351	-117.37545	109.304196688	-0.96900002241	5.85319787061	415.853197871	34.4912	175.2691
99	CI.SAL..BHT	33.2801	-115.98585	110.641435629	-3.55300008217	21.4617255256	431.461725526	34.5175	176.1185
100	CI.SBB2..BHT	34.68844	-117.82424	108.709480597	-0.807500018675	4.87766489217	414.877664892	34.8054	174.7441
101	CI.SBI..BHT	33.48046	-119.02986	108.193217145	-4.03750009337	24.3883244609	434.388324461	33.5252	174.9732
102	CI.SDD..BHT	18.4632	-69.9169	151.948317877	4.52200010458	-27.3149233962	382.685076604	58.306	197.1016
103	CI.SDD..BHT	18.4632	-69.9169	151.948317877	4.52200010458	-27.3149233962	382.685076604	58.306	197.1016
104	CI.SDG..BHT	32.784	-117.13805	109.920562289	0.0	-0.0	410.0	33.7262	175.9871
105	CI.SDR..BHT	32.73561	-116.94241	110.091542521	3.39150007843	-20.4861925471	389.513807453	33.765	176.0798
106	CI.SES..BHT	34.43692	-119.1375	107.784110913	-5.00650011578	30.2415223315	440.241522331	34.1511	174.4398
107	CI.SLA..BHT	35.89095	-117.28332	108.683945567	0.161500003735	-0.975532978435	409.024467022	35.8277	174.247
108	CI.SLH..BHT	33.19269	-116.25399	110.465039374	0.64600001494	-3.90213191374	406.097868086	34.3522	176.0749
109	CI.SMW..BHT	35.01108	-120.40997	106.606100105	-7.10600016434	42.9234510511	452.923451051	34.0914	173.707
110	CI.SNO..BHT	34.03515	-116.80778	109.72782628	-2.26100005229	13.6574616981	423.657461698	34.7346	175.436
111	CI.SPG2..BHT	36.20057	-118.76624	107.454172286	-4.03750009337	24.3883244609	434.388324461	35.4829	173.6012
112	CI.SRI..BHT	33.97875	-120.07886	107.204514798	7.42900017181	-44.874517008	365.125482992	33.4995	174.3546

113	CI.SRT..BHT	35.69235	-117.75051	108.404062111	-0.484500011205	2.9265989353	412.926598935	35.5177	174.2116
114	CI.STC..BHT	34.30302	-119.18676	107.791571766	-5.32950012325	32.1925882883	442.192588288	34.041	174.4935
115	CI.STS..BHT	33.79033	-118.19878	108.736712953	0.0	-0.0	410.0	34.0438	175.0987
116	CI.SVD..BHT	34.10647	-117.09822	109.477773381	0.0	-0.0	410.0	34.6743	175.3008
117	CI.SWS..BHT	32.94508	-115.79988	110.909996194	1.61500003735	-9.75532978435	400.244670216	34.3506	176.3606
118	CI.SYN..BHT	34.60723	-120.0696	107.003695064	-4.52200010458	27.3149233962	437.314923396	33.9356	174.0338
119	CI.TEH..BHT	35.2913	-118.42079	108.038356191	-1.77650004108	10.7308627628	420.730862763	34.997	174.2184
120	CI.TFT..BHT	35.14592	-119.41946	107.32406102	5.49100012699	-33.1681212668	376.831878733	34.5349	173.9679
121	CI.THM..BHT	33.65066	-116.07734	110.433387209	8.88250020542	-53.6543138139	356.345686186	34.7445	175.8876
122	CI.TIN..BHT	37.05422	-118.23009	107.548846006	1.29200002988	-7.80426382748	402.195736173	36.2467	173.2799
123	CI.TOW2..BHT	35.80856	-117.76488	108.350967735	0.0	-0.0	410.0	35.5908	174.1414
124	CI.WAS2..BHT	35.7377	-118.55743	107.776259445	4.52200010458	-27.3149233962	382.685076604	35.249	173.9271
125	CI.WBS..BHT	35.53664	-118.14035	108.164619749	0.0	-0.0	410.0	35.2671	174.1737
126	CI.WES..BHT	32.75904	-115.73161	111.03202552	3.06850007096	-18.5351265903	391.46487341	34.2438	176.4827
127	CI.WGR..BHT	34.51085	-119.27407	107.653055991	-3.7145000859	22.437258504	432.437258504	34.1528	174.3546
128	CI.WMD..BHT	33.03826	-115.58191	111.045188306	-0.96900002241	5.85319787061	415.853197871	34.5018	176.3842
129	CI.WTT2..BHT	33.94867	-118.25539	108.637452354	-3.2300000747	19.5106595687	429.510659569	34.1336	174.9962

Table 2: Data of the 660 km discontinuity

	traces660	latitude660	longitude410	distance660	timeshift660	deltadepth660	absdepth660	mlatitude660	mlongitude660
0	AK.ANM..BHT	64.5646	-165.3732	76.4399725213	-9.85150022783	71.6987057619	731.698705762	39.5691	144.3745
1	AK.BAL..BHT	61.035999	-142.346207	86.5336374226	5.00650011578	-36.4370471905	623.56295281	41.8986	151.4643
2	AK.BARN..BHT	61.059502	-141.662201	86.8610931818	3.87600008964	-28.2093268571	631.790673143	42.0483	151.5694
3	AK.BWN..BHT	64.173203	-149.299103	83.2352181671	1.61500003735	-11.7538861905	648.24611381	41.8695	147.9245
4	AK.CAPN..BHT	60.768299	-151.1539	82.2604431686	1.45350003361	-10.5784975714	649.421502429	40.0974	149.8823
5	AK.CAST..BHT	63.4188	-152.084396	81.9727399495	-2.74550006349	19.9816065238	679.981606524	41.0811	147.9276
6	AK.COLD..BHT	67.226898	-150.203796	82.9679829755	0.0	-0.0	660.0	42.9068	145.5194
7	AK.CUT..BHT	62.4058	-150.262497	82.7500750785	0.0	-0.0	660.0	40.9677	148.9798
8	AK.CYK..BHT	60.082298	-142.487198	86.5484551772	0.64600001494	-4.70155447619	655.298445524	41.4708	152.134
9	AK.DIV..BHT	61.1292	-145.7749	84.8733053266	2.26100005229	-16.4554406667	643.544559333	41.2568	150.7526
10	AK.EYAK..BHT	60.548698	-145.75	84.9068305417	4.36050010084	-31.7354927143	628.264507286	41.0139	151.1646
11	AK.FALS..BHT	54.8564	-163.417603	75.0356490897	0.0	-0.0	660.0	35.2248	149.8925
12	AK.GAMB..BHT	63.775799	-171.703598	73.5767286149	0.0	-0.0	660.0	38.399	143.2888
13	AK.HDA..BHT	64.4091	-146.9482	84.2563016969	0.0	-0.0	660.0	42.3767	148.16
14	AK.JIS..BHT	58.275799	-134.384796	90.9184953808	3.55300008217	-25.858549619	634.141450381	42.5178	154.9477
15	AK.KIAG..BHT	60.9231	-142.360504	86.5367132547	1.77650004108	-12.9292748095	647.07072519	41.8491	151.5449
16	AK.KLU..BHT	61.4924	-145.9227	84.7897530282	-1.77650004108	12.9292748095	672.92927481	41.3816	150.467
17	AK.KTH..BHT	63.5527	-150.923294	82.4978622491	6.4600001494	-47.0155447619	612.984455238	41.3349	148.0613
18	AK.LOGN..BHT	60.824001	-141.004807	87.2031300645	2.42250005602	-17.6308292857	642.369170714	42.0878	151.8616
19	AK.MCK..BHT	63.7318	-148.937302	83.3849445115	0.0	-0.0	660.0	41.7537	148.3066
20	AK.NEA2..BHT	64.5928	-149.0694	83.3439719311	-4.68350010831	34.0862699524	694.086269952	42.0775	147.6617
21	AK.PAX..BHT	62.969898	-145.469894	84.9478140141	0.0	-0.0	660.0	42.0755	149.4809
22	AK.RIDG..BHT	63.7399	-144.8462	85.1946773227	-5.97550013819	43.4893789047	703.489378905	42.4976	149.0124
23	AK.SCM..BHT	61.832001	-147.328995	84.1148253765	-2.90700006723	21.1569951429	681.156995143	41.2583	149.9557
24	AK.SCRK..BHT	63.976101	-143.990494	85.5586185659	1.13050002614	-8.22772033333	651.772279667	42.749	148.9713
25	AK.SLK..BHT	60.5117	-150.223099	82.7067929592	0.0	-0.0	660.0	40.1521	150.2528

26	AK.TRF..BHT	63.4501	-150.2892	82.7761057303	4.68350010831	-34.0862699524	625.913730048	41.4017	148.2538
27	AK.VRDI..BHT	61.227501	-143.454498	85.984964602	0.0	-0.0	660.0	41.7543	151.1216
28	CI.ARV..BHT	35.1269	-118.83009	107.782956097	5.97550013819	-43.4893789047	616.510621095	34.7352	174.1736
29	CI.BAK..BHT	35.34444	-119.104446	107.497233308	0.0	-0.0	660.0	34.7834	173.965
30	CI.BBS..BHT	33.92139	-116.98058	109.635703096	0.807500018675	-5.87694309524	654.123056905	34.5895	175.44
31	CI.BC3..BHT	33.655151	-115.453659	110.91317754	0.0	-0.0	660.0	34.9902	176.0915
32	CI.BEL..BHT	51.837002	20.792	94.2780024179	4.36050010084	-31.7354927143	628.264507286	40.4884	89.4112
33	CI.BEL..BHT	51.837002	20.792	94.2780024179	4.36050010084	-31.7354927143	628.264507286	40.4884	89.4112
34	CI.BHP..BHT	33.99053	-118.36171	108.54021894	2.90700006723	-21.1569951429	638.843004857	34.1237	174.938
35	CI.BLA2..BHT	34.06931	-116.38993	110.037295879	0.32300000747	-2.35077723809	657.649222762	34.9181	175.5556
36	CI.BLC..BHT	34.24356	-118.67312	108.210652217	4.19900009711	-30.5601040952	629.439895905	34.1857	174.699
37	CI.BLY..BHT	44.7488	17.1839	98.4909078357	-3.06850007096	22.3323837619	682.332383762	37.8232	83.8124
38	CI.BLY..BHT	44.7488	17.1839	98.4909078357	-3.06850007096	22.3323837619	682.332383762	37.8232	83.8124
39	CI.BOM..BHT	33.36465	-115.72963	110.808854111	-0.807500018675	5.87694309524	665.876943095	34.6768	176.1586
40	CI.CGO..BHT	36.5504	-117.80295	108.051412291	0.0	-0.0	660.0	36.0731	173.7048
41	CI.CIA..BHT	33.401898	-118.415021	108.702290858	-6.29850014566	45.8401561428	705.840156143	33.6925	175.2265
42	CI.CLT..BHT	34.09284	-117.31687	109.313835193	0.0	-0.0	660.0	34.5825	175.2353
43	CI.COA..BHT	32.86341	-115.12339	111.467429834	-1.45350003361	10.5784975714	670.578497571	34.5561	176.6325
44	CI.CRG..BHT	35.2422	-119.72486	107.056615606	0.0	-0.0	660.0	34.4909	173.8146
45	CI.CTW..BHT	33.67728	-115.87214	110.582031276	5.81400013446	-42.3139902857	617.686009714	34.8426	175.9411
46	CI.CWC..BHT	36.439047	-118.080495	107.88433538	0.0	-0.0	660.0	35.8953	173.6824
47	CI.DEV..BHT	33.93597	-116.57794	94.3169834731	0.0	-0.0	660.0	34.7528	175.5662
48	CI.DEV..BHT	33.93597	-116.57794	94.3169834731	0.0	-0.0	660.0	34.7528	175.5662
49	CI.DJJ..BHT	34.10618	-118.45505	108.427500352	0.0	-0.0	660.0	34.17	174.8454
50	CI.DRE..BHT	46.1733	13.645	100.413574054	-2.09950004855	15.2800520476	675.280052048	39.7306	83.8365
51	CI.DRE..BHT	46.1733	13.645	100.413574054	-2.09950004855	15.2800520476	675.280052048	39.7306	83.8365
52	CI.DSC..BHT	35.14255	-116.10395	109.854111446	0.96900002241	-7.05233171428	652.947668286	35.7715	175.0474
53	CI.EDW2..BHT	34.8811	-117.99388	108.510582143	0.0	-0.0	660.0	34.8747	174.5831
54	CI.ELS2..BHT	33.64907	-117.42604	109.388003839	0.0	-0.0	660.0	34.2311	175.4357

55	CI.ERR..BHT	33.11652	-115.82273	110.828764967	2.26100005229	-16.4554406667	643.544559333	34.4642	176.2612
56	CI.FHO..BHT	34.09355	-116.93588	109.607724158	9.36700021663	-68.1725399047	591.827460095	34.7267	175.3617
57	CI.FIG..BHT	34.72832	-119.98803	107.02658915	-3.39150007843	24.683161	684.683161	34.0474	173.9983
58	CI.FMP..BHT	33.71264	-118.29381	108.689657381	0.0	-0.0	660.0	33.9547	175.1069
59	CI.FOX2..BHT	34.7339	-118.24046	108.373489461	0.0	-0.0	660.0	34.6825	174.5818
60	CI.FUR..BHT	36.46703	-116.86322	101.22532215	0.0	-0.0	660.0	36.3738	174.0433
61	CI.FUR..BHT	36.46703	-116.86322	101.22532215	0.0	-0.0	660.0	36.3738	174.0433
62	CI.GMA..BHT	34.29148	-116.38256	109.960706192	0.0	-0.0	660.0	35.0759	175.4357
63	CI.GMR..BHT	34.78457	-115.65994	110.326733625	0.0	-0.0	660.0	35.6984	175.3925
64	CI.GSC..BHT	35.30177	-116.80574	109.26294293	4.84500011205	-35.2616585714	624.738341429	35.61	174.7338
65	CI.HLL..BHT	34.17643	-118.35967	108.477048767	1.61500003735	-11.7538861905	648.24611381	34.2537	174.8405
66	CI.HMT2..BHT	33.708115	-117.001524	109.696614244	0.0	-0.0	660.0	34.432	175.5476
67	CI.HYS..BHT	34.86532	-117.56975	108.841055037	-4.52200010458	32.9108813333	692.910881333	35.0221	174.7309
68	CI.IDO..BHT	33.79678	-116.22152	110.267887877	-1.93800004482	14.1046634286	674.104663429	34.7918	175.7602
69	CI.IKP..BHT	32.65012	-116.10948	110.776211791	3.39150007843	-24.683161	635.316839	34.02	176.4111
70	CI.ISA..BHT	35.66278	-118.47403	107.86616008	-13.8890003212	101.083421238	761.083421238	35.2291	173.9957
71	CI.JEM..BHT	33.08098	-116.59755	110.237754008	-1.45350003361	10.5784975714	670.578497571	34.1417	176.0176
72	CI.JNH2..BHT	34.448941	-117.95541	108.693783232	3.55300008217	-25.858549619	634.141450381	34.5914	174.8304
73	CI.LCP..BHT	34.73551	-120.27996	106.797930529	0.0	-0.0	660.0	33.9493	173.8953
74	CI.LDF..BHT	35.13066	-115.18416	110.553296737	5.81400013446	-42.3139902857	617.686009714	36.1244	175.3434
75	CI.LFP..BHT	34.30529	-118.48805	108.332669594	-2.42250005602	17.6308292857	677.630829286	34.296	174.7288
76	CI.LGB..BHT	33.9753	-118.14918	108.710687078	0.0	-0.0	660.0	34.1912	175.0181
77	CI.LLS..BHT	33.68447	-117.94304	108.972974128	-2.58400005976	18.8062179048	678.806217905	34.0639	175.2414
78	CI.LRL..BHT	35.47954	-117.68212	108.533139251	3.7145000859	-27.0339382381	632.966061762	35.3993	174.3532
79	CI.MCT..BHT	34.22645	-116.04073	110.247116895	0.0	-0.0	660.0	35.1625	175.5834
80	CI.MGE..BHT	33.81841	-116.36874	110.146216825	0.0	-0.0	660.0	34.7504	175.6995
81	CI.MLAC..BHT	37.63019	-118.83605	106.891096755	-4.68350010831	34.0862699524	694.086269952	36.3992	172.7571
82	CI.MLS..BHT	34.0046	-117.56162	109.877750086	0.0	-0.0	660.0	34.4293	175.2007
83	CI.MLS..BHT	34.0046	-117.56162	109.877750086	0.0	-0.0	660.0	34.4293	175.2007

84	CI.MOP..BHT	34.28096	-118.90469	108.018102245	0.0	-0.0	660.0	34.1275	174.6008
85	CI.MPM..BHT	36.05799	-117.48901	108.467629613	2.90700006723	-21.1569951429	638.843004857	35.8623	174.0866
86	CI.MPP..BHT	34.88848	-119.81362	107.10779165	0.0	-0.0	660.0	34.2186	173.973
87	CI.MSC..BHT	34.03852	-116.64795	109.849865848	0.0	-0.0	660.0	34.7978	175.4871
88	CI.MTG..BHT	33.19915	-116.64727	110.156175829	-0.484500011205	3.52616585714	663.526165857	34.2068	175.9382
89	CI.NBS..BHT	34.78035	-116.55798	109.645038031	5.00650011578	-36.4370471905	623.56295281	35.3473	175.1069
90	CI.NEE2..BHT	34.76759	-114.61881	111.121741797	0.64600001494	-4.70155447619	655.298445524	36.0997	175.7309
91	CI.NJQ..BHT	34.53412	-120.17737	106.944241155	4.36050010084	-31.7354927143	628.264507286	33.8476	174.0351
92	CI.PDE..BHT	34.44199	-118.58215	108.212292797	-7.26750016807	52.8924878571	712.892487857	34.356	174.6244
93	CI.PDM..BHT	34.30336	-114.14152	111.666123279	0.32300000747	-2.35077723809	657.649222762	35.9692	176.1495
94	CI.PMD..BHT	33.64785	-116.37769	110.202045365	0.0	-0.0	660.0	34.627	175.789
95	CI.PSD..BHT	33.82393	-116.55026	110.003935517	-0.64600001494	4.70155447619	664.701554476	34.6848	175.6362
96	CI.PSR..BHT	34.09181	-117.80709	108.93498382	0.0	-0.0	660.0	34.3987	175.0717
97	CI.RUN..BHT	32.97222	-114.97809	111.539294044	0.0	-0.0	660.0	34.6914	176.6223
98	CI.RVR..BHT	33.99351	-117.37545	109.304196688	2.09950004855	-15.2800520476	644.719947952	34.4912	175.2691
99	CI.SAL..BHT	33.2801	-115.98585	110.641435629	-0.807500018675	5.87694309524	665.876943095	34.5175	176.1185
100	CI.SBI..BHT	33.48046	-119.02986	108.193217145	-6.13700014193	44.6647675238	704.664767524	33.5252	174.9732
101	CI.SCI2..BHT	32.9799	-118.54697	108.743046596	12.9200002988	-94.0310895238	565.968910476	33.3468	175.3964
102	CI.SDR..BHT	32.73561	-116.94241	110.091542521	-6.13700014193	44.6647675238	704.664767524	33.765	176.0798
103	CI.SES..BHT	34.43692	-119.1375	107.784110913	0.0	-0.0	660.0	34.1511	174.4398
104	CI.SLB..BHT	33.48519	-115.86643	110.658002721	1.45350003361	-10.5784975714	649.421502429	34.7091	176.0476
105	CI.SMI..BHT	34.03818	-120.35132	106.971662786	-0.807500018675	5.87694309524	665.876943095	33.4452	174.2298
106	CI.SMM..BHT	35.3142	-119.99581	106.824105678	-0.484500011205	3.52616585714	663.526165857	34.4432	173.6857
107	CI.SPF..BHT	34.05933	-118.64614	108.295249445	-1.93800004482	14.1046634286	674.104663429	34.0678	174.8052
108	CI.SPG2..BHT	36.20057	-118.76624	107.454172286	1.29200002988	-9.40310895238	650.596891048	35.4829	173.6012
109	CI.SRI..BHT	33.97875	-120.07886	107.204514798	-9.6900002241	70.5233171428	730.523317143	33.4995	174.3546
110	CI.STC..BHT	34.30302	-119.18676	107.791571766	0.0	-0.0	660.0	34.041	174.4935
111	CI.STS..BHT	33.79033	-118.19878	108.736712953	-1.45350003361	10.5784975714	670.578497571	34.0438	175.0987
112	CI.SVD..BHT	34.10647	-117.09822	109.477773381	-1.93800004482	14.1046634286	674.104663429	34.6743	175.3008

113	CI.SYP..BHT	34.52781	-119.97832	107.101010271	3.87600008964	-28.2093268571	631.790673143	33.9134	174.1063
114	CI.TA2..BHT	34.38203	-117.67822	108.931294886	2.58400005976	-18.8062179048	641.193782095	34.6482	174.9588
115	CI.TFT..BHT	35.14592	-119.41946	107.32406102	-4.36050010084	31.7354927143	691.735492714	34.5349	173.9679
116	CI.THM..BHT	33.65066	-116.07734	110.433387209	0.32300000747	-2.35077723809	657.649222762	34.7445	175.8876
117	CI.TIN..BHT	37.05422	-118.23009	107.548846006	2.74550006349	-19.9816065238	640.018393476	36.2467	173.2799
118	CI.TOR..BHT	33.57526	-116.22584	110.346346254	1.29200002988	-9.40310895238	650.596891048	34.634	175.879
119	CI.TPO..BHT	34.87883	-118.22864	108.331353347	0.807500018675	-5.87694309524	654.123056905	34.7863	174.507
120	CI.VES..BHT	35.84089	-119.08469	107.339600471	0.0	-0.0	660.0	35.1257	173.6993
121	CI.VTV..BHT	34.56065	-117.3296	109.135240696	2.26100005229	-16.4554406667	643.544559333	34.9024	174.9769
122	CI.WAS2..BHT	35.7377	-118.55743	107.776259445	-6.62150015313	48.1909333809	708.190933381	35.249	173.9271
123	CI.WBS..BHT	35.53664	-118.14035	108.164619749	0.0	-0.0	660.0	35.2671	174.1737
124	CI.WES..BHT	32.75904	-115.73161	111.03202552	-0.32300000747	2.35077723809	662.350777238	34.2438	176.4827
125	CI.WGR..BHT	34.51085	-119.27407	107.653055991	0.807500018675	-5.87694309524	654.123056905	34.1528	174.3546
126	CI.WMD..BHT	33.03826	-115.58191	111.045188306	-0.32300000747	2.35077723809	662.350777238	34.5018	176.3842
127	CI.WRC2..BHT	35.9479	-117.65038	108.386555568	2.90700006723	-21.1569951429	638.843004857	35.7276	174.0986
128	CI.WTT2..BHT	33.94867	-118.25539	108.637452354	1.13050002614	-8.22772033333	651.772279667	34.1336	174.9962

Table 3: Data of the CMB

	tracesScS	latitudeScS	longitudeScS	distanceScS	timeshiftScS	deltadepthScS	absdepthScS	mlatitudeScS	mlongitudeScS
0	AK.ANM..BHT	64.5646	-165.3732	76.4399725213	-9.85150022783	-37.2374185878	2853.76258141	39.5691	144.3745
1	AK.BAL..BHT	61.035999	-142.346207	86.5336374226	5.00650011578	18.9239340364	2909.92393404	41.8986	151.4643
2	AK.BARN..BHT	61.059502	-141.662201	86.8610931818	3.87600008964	14.6507876411	2905.65078764	42.0483	151.5694
3	AK.BWN..BHT	64.173203	-149.299103	83.2352181671	1.61500003735	6.10449485046	2897.10449485	41.8695	147.9245
4	AK.CAPN..BHT	60.768299	-151.1539	82.2604431686	1.45350003361	5.49404536542	2896.49404537	40.0974	149.8823
5	AK.CAST..BHT	63.4188	-152.084396	81.9727399495	-2.74550006349	-10.3776412458	2880.62235875	41.0811	147.9276
6	AK.COLD..BHT	67.226898	-150.203796	82.9679829755	0.0	0.0	2891.0	42.9068	145.5194
7	AK.CUT..BHT	62.4058	-150.262497	82.7500750785	0.0	0.0	2891.0	40.9677	148.9798
8	AK.CYK..BHT	60.082298	-142.487198	86.5484551772	0.64600001494	2.44179794019	2893.44179794	41.4708	152.134
9	AK.DIV..BHT	61.1292	-145.7749	84.8733053266	2.26100005229	8.54629279065	2899.54629279	41.2568	150.7526
10	AK.EYAK..BHT	60.548698	-145.75	84.9068305417	4.36050010084	16.4821360962	2907.4821361	41.0139	151.1646
11	AK.FALS..BHT	54.8564	-163.417603	75.0356490897	0.0	0.0	2891.0	35.2248	149.8925
12	AK.GAMB..BHT	63.775799	-171.703598	73.5767286149	0.0	0.0	2891.0	38.399	143.2888
13	AK.HDA..BHT	64.4091	-146.9482	84.2563016969	0.0	0.0	2891.0	42.3767	148.16
14	AK.JIS..BHT	58.275799	-134.384796	90.9184953808	3.55300008217	13.429888671	2904.42988867	42.5178	154.9477
15	AK.KIAG..BHT	60.9231	-142.360504	86.5367132547	1.77650004108	6.71494433551	2897.71494434	41.8491	151.5449
16	AK.KLU..BHT	61.4924	-145.9227	84.7897530282	-1.77650004108	-6.71494433551	2884.28505566	41.3816	150.467
17	AK.KTH..BHT	63.5527	-150.923294	82.4978622491	6.4600001494	24.4179794019	2915.4179794	41.3349	148.0613
18	AK.LOGN..BHT	60.824001	-141.004807	87.2031300645	2.42250005602	9.15674227569	2900.15674228	42.0878	151.8616
19	AK.MCK..BHT	63.7318	-148.937302	83.3849445115	0.0	0.0	2891.0	41.7537	148.3066
20	AK.NEA2..BHT	64.5928	-149.0694	83.3439719311	-4.68350010831	-17.7030350663	2873.29696493	42.0775	147.6617
21	AK.PAX..BHT	62.969898	-145.469894	84.9478140141	0.0	0.0	2891.0	42.0755	149.4809
22	AK.RIDG..BHT	63.7399	-144.8462	85.1946773227	-5.97550013819	-22.5866309467	2868.41336905	42.4976	149.0124
23	AK.SCM..BHT	61.832001	-147.328995	84.1148253765	-2.90700006723	-10.9880907308	2880.01190927	41.2583	149.9557
24	AK.SCRK..BHT	63.976101	-143.990494	85.5586185659	1.13050002614	4.27314639532	2895.2731464	42.749	148.9713
25	AK.SLK..BHT	60.5117	-150.223099	82.7067929592	0.0	0.0	2891.0	40.1521	150.2528

26	AK.TRF..BHT	63.4501	-150.2892	82.7761057303	4.68350010831	17.7030350663	2908.70303507	41.4017	148.2538
27	AK.VRDI..BHT	61.227501	-143.454498	85.984964602	0.0	0.0	2891.0	41.7543	151.1216
28	CI.BEL..BHT	51.837002	20.792	94.2780024179	-0.64600001494	-2.44179794019	2888.55820206	40.4884	89.4112
29	CI.BEL..BHT	34.0006	-115.9982	94.2780024179	-4.68350010831	-17.7030350663	2873.29696493	35.0211	175.7222
30	CI.BLY..BHT	33.7503	-114.52375	98.4909078357	0.0	0.0	2891.0	35.4261	176.3422
31	CI.BLY..BHT	44.7488	17.1839	98.4909078357	-2.90700006723	-10.9880907308	2880.01190927	37.8232	83.8124
32	CI.BLY..BHT	33.7503	-114.52375	98.4909078357	0.0	0.0	2891.0	35.4261	176.3422
33	CI.DEV..BHT	33.93597	-116.57794	94.3169834731	0.0	0.0	2891.0	34.7528	175.5662
34	CI.DEV..BHT	33.93597	-116.57794	94.3169834731	0.0	0.0	2891.0	34.7528	175.5662
35	CI.FUR..BHT	36.46703	-116.86322	101.22532215	4.03750009337	15.2612371262	2906.26123713	36.3738	174.0433
36	CI.FUR..BHT	36.46703	-116.86322	101.22532215	0.0	0.0	2891.0	36.3738	174.0433

B Jpyter-notebook

Comparison of Real Event and Simulation

Importing and defining functions:

```
from obspy.clients.fdsn.mass_downloader import CircularDomain,
Restrictions, MassDownloader
from obspy.core import UTCDateTime
from obspy import read_inventory, read_events
from obspy import read
from obspy.geodetics import locations2degrees
from obspy import Stream
from obspy.taup import TauPyModel
from obspy.geodetics.base import gps2dist_azimuth
from collections import defaultdict
from obspy.signal.cross_correlation import correlate
from obspy.signal.cross_correlation import xcorr_max
from mpl_toolkits.basemap import Basemap
from numpy import mean

import os
import glob
import matplotlib.pyplot as plt
import numpy as np
import csv
import matplotlib.ticker as ticker
import math
import pandas as pd
import matplotlib.patches as patches
```

```
def stationloc(x):
    for i in range(len(sta)):
        if x == sta[i].code:
            lat = sta[i].latitude
            lon = sta[i].longitude
    return lat,lon
```

```
def sort_array(inputarr):
    in_arr = np.array(inputarr)
    out_arr = np.argsort(in_arr)
    sorted_array = in_arr[out_arr]
    return sorted_array

def traveltimes(arrivals):
    phase_list = []
    time_list = []
    for a in range(len(arrivals)):
        arr = arrivals[a]
        ph_arr = arr.name
        time_arr = arr.time
        phase_list.append(ph_arr)
        time_list.append(time_arr)
    return phase_list,time_list

def phasepoints(times,time_list_a):
    index_list_a = []
    for g in range(len(time_list_a)):
        index_list =find_index(times,time_list_a[g])
        index_list_a.append(index_list)
    return index_list_a

def find_index(array, value):
    array = np.asarray(array)
    idx = (np.abs(array - value)).argmin()
    return idx
```

Event Parameters

```
# Determining event parameters
originTime = UTCDateTime('2017-04-28T20:23:17Z')
```

```
startTimeTrim=UTCDateTime('2017-04-28T20:23:20Z')    # needed for
    processing, all datas have to be recorded for the same time
endTimeTrim = startTimeTrim + 3300                    # recording
    goes 55 min

event_lat = 5.49  # event latitude
event_lon = 124.89  # event longitude
event_depth = 31.35  # event depth
```

```
# List of station filenames

stations_list =sorted(glob.glob("stationsPhil2017/*.xml"))

# List of waveform filenames

waveforms_list = sorted(glob.glob("waveformsPhil2017/*.mseed"))

# Inventory

net = [] #network

for filename in sorted(glob.glob("stationsPhil2017/*.xml")):
    net += read_inventory(filename)
```

```
print(len(waveforms_list))
```

```
4866
```

```
# Stations and Channels

sta = [] # station
cha = [] # channel
```

```
for i in range(len(net)):
    sta += net[i]


for j in range(len(sta)):
    cha += sta[j]
```

```
# Create stream for processing and further use, like plotting

root = 'waveformsPhil2017/*.mseed'
stream =[]

for  filename in sorted(glob.glob(root)):
    stream+= read(filename)  # create a stream with all the
       traces


# with st your stream with traces:

traces_real = []  # initiating, vector with all processed traces
simulation_sampling = 6.19195032119751 # sampling rate is 6.2Hz,
   a sample every 0.16s


# initiating, vectors with processed traces for each polarization
    direction
traces_1N = []
traces_1E = []
traces_1Z = []

inve_list = []

tr_E = (read(waveforms_list[0]))[0].copy()
```

```
tr_N = (read(waveforms_list[1]))[0].copy()
tr_Z = (read(waveforms_list[2]))[0].copy()

# Processing the data
for j in range(len(waveforms_list)):
    st = read(waveforms_list[j])
    tr = st[0].copy()
    for i in range(len(stations_list)):
        if sta[i].code == tr.stats.station:
            inve = read_inventory(stations_list[i])
            #tr.remove_response(inventory=inve, output='DISP')
            tr.resample(simulation_sampling) # all traces need
               the same sampling frequency
            tr.stats["coordinates"] = {} # add the coordinates to
                your dictionary, needed for the section plot
            tr.stats["coordinates"]["latitude"] = (sta[i]).
               latitude
            tr.stats["coordinates"]["longitude"] = (sta[i]).
               longitude
            tr_filt = tr.copy()
            tr_filt.filter('bandpass', freqmin=1e-02, freqmax=8e
               -02, corners=2, zerophase=True) # 0.01-0.08Hz or
               12.5-100s
            tr_filt.normalize()
            tr_filt.trim(startTimeTrim, endTimeTrim) # recording
               goes exactly 55 min

            # Filling the vectors, separeted by channel
            if tr_filt.stats.channel == 'BHN' or tr_filt.stats.
               channel =='BH2':
                tr_N = tr_filt.copy()
                traces_1N.append(tr_filt)
                inve_list.append(inve)
```

```
            elif tr_filt.stats.channel == 'BHE' or tr_filt.stats.
               channel =='BH1':
                tr_E = tr_filt.copy()
                traces_1E.append(tr_filt)
            elif  tr_filt.stats.channel == 'BHZ':
                tr_Z = tr_filt.copy()
                traces_1Z.append(tr_filt)

            # A vector with all traces
            traces_real.append(tr_filt)
```

```
# initiating new vectors with all the same length and the same
   stations
traces_N = []
traces_E = []
traces_Z = []

i=0
j=0
k=0
# while loop kicks out all traces that do not have all three
   channels
while i < len(traces_1N) and j < len(traces_1E) and k < len(
   traces_1Z):
    if traces_1N[i].stats.station == traces_1E[j].stats.station
       == traces_1Z[k].stats.station:
        traces_N.append(traces_1N[i])
        traces_E.append(traces_1E[j])
        traces_Z.append(traces_1Z[k])
        i=i+1
        j=j+1
        k=k+1
    elif traces_1N[i].stats.station < traces_1E[j].stats.station:
```

```
        i=i+1
    elif traces_1N[i].stats.station < traces_1Z[k].stats.station:
        i=i+1
    else:
        k=k+1
```

```
# Appending different information to the traces
starttime_N = []
endtime_N = []
starttime_E = []
endtime_E = []
baz = []
time_N = []
time_E = []

a = len(traces_N)
b = len(traces_E)
s = min(a,b)

for i in range(s):
    distance, forward_az, back_az = gps2dist_azimuth(event_lat,
       event_lon, (traces_N[i]).stats.coordinates.latitude,
            traces_N[i].stats.coordinates.longitude)
    start = traces_N[i].stats.starttime
    starttime_N.append(start)
    end = traces_N[i].stats.endtime
    endtime_N.append(end)
    time = endtime_N[i] - starttime_N[i]
    time_N.append(time)
    start = traces_E[i].stats.starttime
    starttime_E.append(start)
    end = traces_E[i].stats.endtime
    endtime_E.append(end)
```

```
    time = endtime_E[i] - starttime_E[i]
    time_E.append(time)
    baz.append(back_az)
```

```
#for i in range(len(traces_N)):
    #print(traces_N[i])
```

```
## Create an empty vector named streams
## streams is a Stream and every element of streams is a Stream
   with two traces
## rotates the N and E traces to R and T traces
streams = []

a = len(traces_N)
b = len(traces_E)
s = min(a,b)

for i in range(len(traces_N)):
    for j in range(len(traces_E)):
        if traces_N[i].stats.station == traces_E[j].stats.station
            and time_N[i] == time_E[j]:
            stream = Stream(traces=[traces_N[i], traces_E[j]])
            stream.rotate(method='NE->RT',inventory=inve_list[i],
               back_azimuth = baz[i])
            streams.append(stream)
```

```
traces_R = []
traces_T1 = []

# spliting up the streams vector and separates the BHT and BHR
   channel
for i in range(len(streams)):
    if streams[i][0].stats.channel == 'BHR':
        traces_R.append(streams[i][0])
```

```
    if streams[i][1].stats.channel == 'BHT':
        traces_T1.append(streams[i][1])
```

```
# converting all transverse traces to sac format
for i in traces_T1:
    i.write(i.id + '.sac', format='SAC',flush_headers=True)
```

```
print(len(traces_T1))
print(len(traces_R))
```

```
481
481
```

```
# Creating a Table with the all the stations latitude and
   longitude. For a Basemap plot. Export it as csv file.
stalat = []
stalon = []

for i in range(len(traces_T1)):
    stalat.append(traces_T1[i].stats.coordinates.latitude)
    stalon.append(traces_T1[i].stats.coordinates.longitude)

df_station = {'stalat': stalat, 'stalon': stalon}
dfstation = pd.DataFrame(data=df_station)

dfstation.to_csv("StationLatLon.csv")
```

Simulation seismograms

```
# SIMULATION

# Loading seismogram file names

filenames_topo = sorted(glob.glob('evMindanao_full_sh/*MXT*sac'))
```

```
print(len(filenames_topo))
```

```
400
```

```
# Settings of evaluation in Taup, needed if we want to plot the
    arrival tiem of phases named in phasse_list_T

m = TauPyModel(model="prem")

#phase_list_T =['S','SS','SSS','ScS','Sdiff','Sv410s','Sv660s','
    Sv410S','Sv660S','S^410S','S^660S',
#                'ScSScS','SSv410s','SSv410S','SSv660s','SSv660S
    ','SS^410S','SS^660S','ScS^410ScS','ScS^660ScS',
#                'ScS^410S','ScS^660S','SKS','sSKS','SKIKS','
    sSKIKS','SKKS','sSdiff','SKIKKIKS','SKSSKS','SKIKSSKIKS']

#phase_list_T =['P','PP','PPP','PcP','PKIKP','PKP','pPKP','pPKIKP
    ','PKKP','pPdiff','PKIKKIKP','PKPPKP','PKIKPPKIKP',
#                'Pdiff','P410P','P660P','Pv660P','Pv410P','P^660P
    ','P^410P','PKP^410P','PKP^660P','PPv410P',
#                'PPv660P','PP^410P','PP^660P','PcP^410PcP','PcP
    ^660PcP','PcP^410P','PcP^660P']

phase_list_T = ['SS', 'ScS', 'S^410S', 'S^660S']
colors = ["r", "g", "y", "b"]
```

```
# Read Seismograms

distance = []
seismograms = []
traces_sim1 = []
difference = []
```

```
time_list_a = []
diff_list_a = []
dist_list_a = []

seis = len(filenames_topo)

for f in range(seis):
    st = read(filenames_topo[f]) # seismogram without topography
    tr = (st[0]).copy()                    # trace without
       topography
    seismograms.append(tr)

# Processing the synthtic data, the same way as the real data
for f in range(len(traces_T1)):
    network = traces_T1[f].stats.network
    station = traces_T1[f].stats.station
    for i in range(len(seismograms)):
        # Making sure that the all traces in the synthtic data
           have an exact corresponding real trace
        # Network and station has to be the same in real (
           traces_T1) and syn (seismograms)
        if seismograms[i].stats.network == network and
           seismograms[i].stats.station == station:
            tr = seismograms[i].copy()

            # Determine distance
            station_lat, station_lon = stationloc(tr.stats.
               station) # gives station latitude and longitude for
                each trace
            dist = locations2degrees(event_lat, event_lon,
               station_lat, station_lon) #epicentral distance for
               each station
            distance.append(dist)
```

```
            tr.resample(simulation_sampling)
            tr.stats["coordinates"] = {} # add the coordinates to
                your dictionary,needed for the section plot
            tr.stats["coordinates"]["latitude"] = station_lat
            tr.stats["coordinates"]["longitude"] = station_lon
            tr_filt = tr.copy()
            tr_filt.filter('bandpass', freqmin=1e-02, freqmax=8e
               -02, corners=2, zerophase=True)
            tr_filt.normalize()
            tr_filt.trim(startTimeTrim, endTimeTrim)

            # all transverse traces of the synthtic data
            traces_sim1.append(tr_filt)
```

```
print(len(traces_sim1))
#for i in range(len(traces_sim1)):
    #print(traces_sim1[i])
```

```
269
```

```
print(len(traces_T1))
#for i in range(len(traces_T1)):
    #print(traces_T1[i])
```

```
481
```

```
traces_T = []
traces_sim = []

# Cuting the real traces vector to the length of the synthetic
   traces vector
i=0
j=0
```

```
# Needed to make sure that network and station correlates
while i < len(traces_T1) and j < len(traces_sim1):
    if traces_T1[i].stats.network == traces_sim1[j].stats.network
        and traces_T1[i].stats.station == traces_sim1[j].stats.
       station:
        traces_T.append(traces_T1[i])
        traces_sim.append(traces_sim1[j])
        i=i+1
        j=j+1
    elif traces_T1[i].stats.network < traces_sim1[j].stats.
       network or traces_T1[i].stats.network == traces_sim1[j].
       stats.network and traces_T1[i].stats.station < traces_sim1[
       j].stats.station:
        i=i+1
    else:
        j=j+1
```

```
for i in range(len(traces_sim)):

    # Trace Data
    tr_r = (traces_T[i]).data # tr_r stores the sample points of
       real traces
    tr_s = (traces_sim[i]).data # tr_s of syn traces
    if (len(tr_r) < 20434):
        ns = len(tr_r)
    else:
        ns = 20434  # number of samples in real trace seismograms
            after resampling, here all traces have 20434 smple
           points
    tr_r_c = tr_r[0:ns]
    tr_s_c = tr_s[0:ns]
    diffe = tr_r_c - tr_s_c # is needed when we want to plot
```

```
        difference of real and syn trace
    difference.append(diffe)

    # Determine arrivals of ScS, S410S, S660S for every
        epicentral distance (distance[i])
    arrivals = m.get_ray_paths(distance_in_degree=distance[i],
        source_depth_in_km=event_depth, phase_list=phase_list_T)

    # Arrays of seismic phase arrivals
    phase_list, time_list = traveltimes(arrivals)
    times = (tr.times())
    time_list_a.append(float(time_list[0]))
    dist_list_a.append(float(distance[i]))
```

```
#for i in range(len(traces_T)):
    #print(traces_T[i])
    #print(traces_sim[i])
```

```
print(len(traces_T))
print(len(traces_sim))
```

```
269
269
```

```
# storage for traveltimes
distances = defaultdict(list)
ttimes = defaultdict(list)



# loop over distances
for dist in np.linspace(70, 115, 30):
    # get traveltimes
    arrivals = m.get_travel_times(distance_in_degree=dist,
                                  source_depth_in_km=31.35,
```

```
                                        phase_list=phase_list_T)
    for arr in arrivals:
        distances[arr.name].append(dist)
        ttimes[arr.name].append(arr.time)


# Plot real waveforms, Record section
stream = Stream(traces_T)
stream.plot(type='section',dist_degree=True, orientation='
   horizontal', ev_coord=(event_lat,event_lon), handle=True)

# Plotting colorful dots
for color, phase in zip(colors, phase_list_T):
    plt.scatter(ttimes[phase], distances[phase], s=10, color=
       color, label=phase)

plt.title("Real data record section of earthquake event at
   28.04.2017")
plt.ylabel("Epicentral distance [°]")
plt.xlabel("Time since event [s]")
plt.legend(loc="upper right")
plt.xlim(1200,2500)
plt.ylim(70,115)

plt.savefig('Figures/RecordSectionReal.pdf')
```

```
# Plot Simulation Waveforms, Record Section

stream = Stream(traces_sim)
stream.plot(type='section',dist_degree=True, orientation='
   horizontal', ev_coord=(event_lat,event_lon), handle=True)

# Plotting colorful dots
```

```
for color, phase in zip(colors, phase_list_T):
    plt.scatter(ttimes[phase], distances[phase], s=10, color=
       color, label=phase)

plt.title("Synthetic data record section of earthquake event at
   28.04.2017")
plt.ylabel("Epicentral distance [°]")
plt.xlabel("Time since event [s]")
plt.legend(loc="upper right")
plt.xlim(1200,2500)
plt.ylim(70,115)

plt.savefig('Figures/RecordSectionSyn.pdf')
```

```
# Plotting differences of reals and corresponding synthetic trace

fig,ax = plt.subplots(figsize=(15,20))

# difference contains the 20434 sample points that make a trace
# distance: epicentral distance
for d,y in zip(difference,distance):
    x = d + y
    ax.plot(x)

ax.set_xlim(1200,2500)
ax.set_ylim(70,115)
ax.set_title('Record section of difference between real and
   synthetic trace')
ax.set_xlabel('Time since event [s]')
ax.set_ylabel('Epicentral distance [°]')

plt.savefig('Figures/RecordSectionDifference.pdf')
```

```
# Calculating arrival time based on prem for precursors, 410 and
    660
model = TauPyModel(model="prem")
phase_list=["S^410S", "S^660S"]

# initiating vectors that only contain the arrival time numbers,
    needed for time winows
arrivalsS410S = []
arrivalsS660S = []
for i in range(len(traces_T)):
    arrivals = model.get_travel_times(source_depth_in_km=31.35,
                                      distance_in_degree=distance[i],
                                          phase_list=phase_list)
    arr440 = arrivals[1]
    arr660 = arrivals[0]
    arrivalsS410S.append(arr440.time)
    arrivalsS660S.append(arr660.time)

#print(arrivalsS410S)
#print(arrivalsS660S)
#print(len(arrivalsS410S))
#print(len(arrivalsS660S))
```

```
# calculating arrival time based on prem for ScS
model = TauPyModel(model="prem")
phase_list_2=["ScS"]

# initiating vector that only contain the arrival time numbers,
    needed for time windows
arrivalsScS = []
traces_RealScS = [] # we need to have vectors that only contain
    the traces from traces_T with  epicentral distance < 105
traces_SynScS = []
```

```
distance_AllScS = []
for i in range(len(traces_T)):
    if distance[i] < 105:
        stationnameReal = traces_T[i]
        stationnameSyn = traces_sim[i]
        arrivals = model.get_travel_times(source_depth_in_km
           =31.35,
                                  distance_in_degree=distance[i],
                                      phase_list=phase_list_2)
        arrScS = arrivals[0]
        arrivalsScS.append(arrScS.time)
        traces_RealScS.append(stationnameReal)
        traces_SynScS.append(stationnameSyn)
        distance_AllScS.append(distance[i])

#print(arrivalsScS)
#print(len(arrivalsScS))
#print(len(traces_RealScS))
#print(len(traces_SynScS))
#print(len(distance_AllScS))
```

Correlate Synthetic and Real Traces and Filter

```
# Calculating time window for precursors, +-50s
timewindowMin410 = []
timewindowMax410 = []

timewindowMin660 = []
timewindowMax660 = []

for i in range(len(arrivalsS410S)):
    Min410 = arrivalsS410S[i] - 50
    Max410 = arrivalsS410S[i] + 50
    timewindowMin410.append(Min410)
```

```
    timewindowMax410.append(Max410)

    Min660 = arrivalsS660S[i] - 50
    Max660 = arrivalsS660S[i] + 50
    timewindowMin660.append(Min660)
    timewindowMax660.append(Max660)

#print(timewindowMin410)
#print(timewindowMax410)

#print(timewindowMin660)
#print(timewindowMax660)
```

```
# Calculating time window for ScS, +-50s
timewindowMinScS = []
timewindowMaxScS = []

for i in range(len(arrivalsScS)):
    MinScS = arrivalsScS[i] - 50
    MaxScS = arrivalsScS[i] + 50
    timewindowMinScS.append(MinScS)
    timewindowMaxScS.append(MaxScS)

#print(timewindowMinScS)
#print(timewindowMaxScS)

#print(len(timewindowMinScS))
#print(len(timewindowMaxScS))
```

```
dt = 1/simulation_sampling # time between sampling points for
    shift calculation

# Correlation for 410 window, shift = 100
corr410 = []
```

```
time_shift410 = []
traces_T410 = []
distance410 = []
latitude410 = []
longitude410 = []
traces_Tcorr = []
traces_simcorr = []

for i in range(len(traces_T)):
    c410 = correlate(traces_T[i][int(timewindowMin410[i]):int(
       timewindowMax410[i])],traces_sim[i][int(timewindowMin410[i
       ]):int(timewindowMax410[i])], shift=100)
    corr410.append(c410) #append the correlations for each
       corresponding traces
    shift, value = xcorr_max(c410)
    if value > 0.5:
        shift410 = shift*dt
        time_shift410.append(shift410)
        traces_T410.append(traces_T[i].id)
        distance410.append(distance[i])
        latitude410.append(traces_T[i].stats.coordinates.latitude
           )
        longitude410.append(traces_T[i].stats.coordinates.
           longitude)
        traces_Tcorr.append(traces_T[i])
        traces_simcorr.append(traces_sim[i])

#print(len(time_shift410))
print(len(traces_T410))
#print(len(distance410))
#print(len(latitude410))
#print(len(longitude410))
```

```
#for i in range(len(traces_T410)):
 #    print(traces_T410[i])
  #   print(latitude410[i])
   # print(longitude410[i])
    #print(distance410[i])
    #print(time_shift410[i])
```

```
# Correlation for 660 window
corr660 = []
time_shift660 = []
traces_T660 = []
distance660 = []
latitude660 = []
longitude660 = []
for i in range(len(traces_T)):
    c660 = correlate(traces_T[i][int(timewindowMin660[i]):int(
       timewindowMax660[i])],traces_sim[i][int(timewindowMin660[i
       ]):int(timewindowMax660[i])], shift=100)
    corr660.append(c660) #append the correlations for each
       corresponding traces
    shift, value = xcorr_max(c660)
    if value > 0.5:
        shift660 = shift*dt
        time_shift660.append(shift660)
        traces_T660.append(traces_T[i].id)
        distance660.append(distance[i])
        latitude660.append(traces_T[i].stats.coordinates.latitude
           )
        longitude660.append(traces_T[i].stats.coordinates.
           longitude)

#print(len(time_shift660))
print(len(traces_T660))
```

```
#print(len(distance660))
#print(len(latitude660))
#print(len(longitude660))
```

```
#for i in range(len(traces_T660)):
 #    print(traces_T660[i])
  #   print(latitude660[i])
   # print(longitude660[i])
    #print(distance660[i])
    #print(time_shift660[i])
```

```
# Correlation for ScS window
corrScS = []
time_shiftScS = []
traces_TScS = []
distanceScS = []
latitudeScS = []
longitudeScS = []
for i in range(len(traces_RealScS)):
    cScS = correlate(traces_RealScS[i][int(timewindowMin660[i]):
       int(timewindowMax660[i])],traces_SynScS[i][int(
       timewindowMin660[i]):int(timewindowMax660[i])], shift=100)
    corrScS.append(cScS) #append the correlations for each
       corresponding traces
    shift, value = xcorr_max(cScS)
    if value > 0.5:
        shiftScS = shift*dt
        time_shiftScS.append(shiftScS)
        traces_TScS.append(traces_RealScS[i].id)
        distanceScS.append(distance_AllScS[i])
        latitudeScS.append(traces_RealScS[i].stats.coordinates.
           latitude)
        longitudeScS.append(traces_RealScS[i].stats.coordinates.
           longitude)
```

```
#print(len(time_shiftScS))
print(len(traces_TScS))
#print(len(distanceScS))
#print(len(latitudeScS))
#print(len(longitudeScS))
```

```
#for i in range(len(traces_TScS)):
 #    print(traces_TScS[i])
  #   print(latitudeScS[i])
   #  print(longitudeScS[i])
    #print(distanceScS[i])
    #print(time_shiftScS[i])
```

```
# Calculating the depth variation from the time shift
Vs_410 = 4.93 # km/s
Vs_660 = 5.94 # km/s
Vs_ScS = 7.2
theta = 20
theta_ScS = 75

r = 6371-2981 # km, radius to CMB
eta = 479.03 # s/rad, vertical ray param
p = 478.87813 # s/rad, ray param for CMB without perturbations

#time_shift410(j) = (-2)*dh_410(j)*cos(theta)/Vs_410 # s
#time_shift660(j) = (-2)*dh_660(j)*cos(theta)/Vs_660 # s

ddepth410 = []
for i in range(len(time_shift410)):
    dh_410 = time_shift410[i]*Vs_410/((-2)*math.cos(theta))
    ddepth410.append(dh_410)

ddepth660 = []
```

```
for i in range(len(time_shift660)):
    dh_660 = time_shift660[i]*Vs_660/((-2)*math.cos(theta))
    ddepth660.append(dh_660)

ddepthScS = []
for i in range(len(time_shiftScS)):
    dh_ScS = -time_shiftScS[i]*Vs_ScS/((-2)*math.cos(theta_ScS))
    #dh_ScS = -dr_ScS
    ddepthScS.append(dh_ScS)
```

```
# Calculating absolute depth for each phase
absdepth410 = []
for i in range(len(time_shift410)):
    depth410 = 410 + ddepth410[i]
    absdepth410.append(depth410)

absdepth660 = []
for i in range(len(time_shift660)):
    depth660 = 660 + ddepth660[i]
    absdepth660.append(depth660)

absdepthScS = []
for i in range(len(time_shiftScS)):
    depthScS = 2891 + ddepthScS[i]
    absdepthScS.append(depthScS)
```

```
# Average value for the three discontnuities for all data points
meandepth410 = mean(absdepth410)
meandepth660 = mean(absdepth660)
meandepthScS = mean(absdepthScS)

print(meandepth410)
print(meandepth660)
print(meandepthScS)
```

```
# Read a csv file with the mid points latitude and longitude
# 410
df4 = pd.read_csv ('410DataBaseMid.csv')

mlatitude410 = df4['mlt'] # vector with the latitude from the csv
    file
mlongitude410 = df4['mln'] # vector with the longitude from the
   csv file

# 660
df6 = pd.read_csv ('660DataBaseMid.csv')

mlatitude660 = df6['mlt']
mlongitude660 = df6['mlon']

# ScS
dfS = pd.read_csv ('ScSDataBaseMid.csv')

mlatitudeScS = dfS['mlt']
mlongitudeScS = dfS['mln']
```

```
# Database for 410 discontinuity
S410S = {'traces410': traces_T410, 'latitude410': latitude410, '
   longitude410': longitude410, 'distance410': distance410, '
   timeshift410': time_shift410, 'deltadepth410': ddepth410, '
   absdepth410': absdepth410, 'mlatitude410': mlatitude410, '
   mlongitude410': mlongitude410}
df410 = pd.DataFrame(data=S410S)
#print(df410)

df410.to_csv("410DataBase.csv")
```

```
# Database for 660 discontinuity
S660S = {'traces660': traces_T660, 'latitude660': latitude660, '
   longitude410': longitude660, 'distance660': distance660, '
   timeshift660': time_shift660, 'deltadepth660': ddepth660, '
   absdepth660': absdepth660, 'mlatitude660': mlatitude660, '
   mlongitude660': mlongitude660}
df660 = pd.DataFrame(data=S660S)
#print(df660)

df660.to_csv("660DataBase.csv")
```

```
# Database for ScS discontinuity
ScS = {'tracesScS': traces_TScS, 'latitudeScS': latitudeScS, '
   longitudeScS': longitudeScS, 'distanceScS': distanceScS, '
   timeshiftScS': time_shiftScS, 'deltadepthScS': ddepthScS, '
   absdepthScS': absdepthScS, 'mlatitudeScS': mlatitudeScS, '
   mlongitudeScS': mlongitudeScS}
dfScS = pd.DataFrame(data=ScS)
#print(dfScS)

dfScS.to_csv("ScSDataBase.csv")
```

```
# Trace Example One by One Comparison

i=11 # selected 11 element of traces_Tcorr, because of very high
   correlation

t1 = (traces_Tcorr[i].data)
t2 = (traces_simcorr[i].data)

# Calculating the colorful dots
model = TauPyModel(model="prem")
phase_list=["S^410S", "S^660S", "ScS", "SS"]
```

```
arrivals = model.get_travel_times(source_depth_in_km=31.35,
                                  distance_in_degree=distance410
                                     [11], phase_list=phase_list)
arr410sta11 = arrivals[2].time/0.16
arr660sta11 = arrivals[1].time/0.16
arrScSsta11 = arrivals[0].time/0.16
arrSSsta11 = arrivals[3].time/0.16

# lower left corner of the boxes that we will plot
lb410 = arr410sta11-(50/0.16)
lb660 = arr660sta11-(50/0.16)
lbScS = arrScSsta11-(50/0.16)
lbSS = arrSSsta11-(50/0.16)

# defining the time window for each phase
rect410 = patches.Rectangle((lb410, -0.75), 625, 1.5, linewidth
   =1, edgecolor='y', facecolor='none')
rect660 = patches.Rectangle((lb660, -0.75), 625, 1.5, linewidth
   =1, edgecolor='b', facecolor='none')
rectScS = patches.Rectangle((lbScS, -0.75), 625, 1.5, linewidth
   =1, edgecolor='g', facecolor='none')
rectSS = patches.Rectangle((lbSS, -0.75), 625, 1.5, linewidth=1,
   edgecolor='r', facecolor='none')

fig, ax = plt.subplots(figsize=(20,10))
plt.plot(t1,label='real') # plot real trace
plt.plot(t2,label='sim') # plot syn trace
# plot the colorful dots
plt.scatter(arr410sta11,0, color="y", label=phase_list[0])
plt.scatter(arr660sta11,0, color="b", label=phase_list[1])
plt.scatter(arrScSsta11,0, color="g",label=phase_list[2])
plt.scatter(arrSSsta11,0, color="r", label=phase_list[3])
# plot time window
```

```
ax.add_patch(rect410)
ax.add_patch(rect660)
ax.add_patch(rectScS)
ax.add_patch(rectSS)

plt.title("Comparison␣of␣real␣data␣trace␣and␣synthtic␣data␣trace"
    )
plt.ylabel("Amplitude␣normalized")
plt.xlabel("Sampling␣points")

plt.xlim(1200/0.16,2500/0.16)
plt.ylim(-1,1)
plt.legend()

#plt.savefig('Figures/TraceRealSim.pdf')
```

```
# Plotting one single trace, transversal component
```

```
trTReal = Stream(traces_T[0])
print(trTReal)
trTReal.plot(outfile='Figures/OneTraceReal.pdf')
```

```
trTSyn = Stream(traces_sim[0])
print(trTSyn)
trTSyn.plot(outfile='Figures/OneTraceSyn.pdf')
```

References

Bagley, B., & Revenaugh, J. (2008). Upper mantle seismic shear discontinuities of the pacific. *Journal of Geophysical Research: Solid Earth*, *113*(B12).

Bai, L., Zhang, Y., & Ritsema, J. (2012). An analysis of *SS* precursors using spectral-element method seismograms. , *188*, 293-300. doi: 10.1111/j.1365-246X.2011.05256.x

Beniest, A. (2017). *From continental rifting to conjugate margins : insights from analogue and numerical modelling* (Unpublished doctoral dissertation).

Crotwell, H. P., Owens, T. J., & Ritsema, J. (n.d.). The TauP ToolKit: Flexible Seismic Travel-Time and Raypath Utilities. *Seismological Research Letters*.

Deuss, A. (2007). Seismic observations of transition-zone discontinuities beneath hotspot locations. *Special Papers-Geological Society of America*, *430*, 121.

Deuss, A. (2009). Global observations of mantle discontinuities using ss and pp precursors. *Surveys in geophysics*, *30*(4-5), 301–326.

Dziewonski, A. M., & Anderson, D. L. (1981). Preliminary reference earth model. *Physics of the earth and planetary interiors*, *25*(4), 297–356.

Flanagan, M., & Shearer, P. (1999). A map of topography of 410-km discontinuity from *PP* precursors. , *26*(5), 549-552.

Houser, C., & Williams, Q. (2010). Reconciling pacific 410 and 660 km discontinuity topography, transition zone shear velocity patterns, and mantle phase transitions. *Earth and Planetary Science Letters*, *296*(3-4), 255–266.

Komatitsch, D., & Tromp, J. (1999). Introduction to the spectral element method for three-dimensional seismic wave propagation. , *139*(3), 806-822. doi: 10.1046/j.1365-246x.1999.00967.x

Komatitsch, D., & Tromp, J. (2002a). Spectral-element simulations of global seismic wave propagation-II. 3-D models, oceans, rotation, and self-gravitation. , *150*(1), 303-318. doi: 10.1046/j.1365-246X.2002.01716.x

Komatitsch, D., & Tromp, J. (2002b). Spectral-element simulations of global seismic wave propagation-I. Validation. , *149*(2), 390-412. doi: 10.1046/j.1365-246X.2002.01653.x

Koroni, M., Bozdağ, E., Paulssen, H., & Trampert, J. (2017). Sensitivity analysis of seismic waveforms to upper-mantle discontinuities using the adjoint method. , *210*, 1965-1980.

Koroni, M., Paulssen, H., & Trampert, J. (2019). Sensitivity kernels of pp precursor traveltimes and their limitations for imaging topography of discontinuities. *Geophysical Research*

Letters, *46*(2), 698-707. doi: 10.1029/2018GL081592

Koroni, M., & Trampert, J. (2016). The effect of topography of upper mantle discontinuities on *SS* precursors. , *204*, 667-681.

Koroni, M., & Trampert, J. (2021, 03). Imaging global mantle discontinuities: a test using full-waveforms and adjoint kernels. *Geophysical Journal International*, *226*(3), 1498-1516. Retrieved from `https://doi.org/10.1093/gji/ggab119` doi: 10.1093/gji/ggab119

Lessing, S., Thomas, C., Saki, M., Schmerr, N., & Vanacore, E. (2015a). On the difficulties of detecting pp precursors. *Geophysical Journal International*, *201*(3), 1666–1681.

Lessing, S., Thomas, C., Saki, M., Schmerr, N., & Vanacore, E. (2015b, 04). On the difficulties of detecting PP precursors. *Geophysical Journal International*, *201*(3), 1666-1681. Retrieved from `https://doi.org/10.1093/gji/ggv105` doi: 10.1093/gji/ggv105

Lindsey, N. J., Rademacher, H., & Ajo-Franklin, J. B. (2020). On the broadband instrument response of fiber-optic das arrays. *Journal of Geophysical Research: Solid Earth*, *125*(2), e2019JB018145.

Revenaugh, J., & Jordan, T. (1991c). Mantle layering from ScS reverberations. , *96*(B12), 19,781-19,810.

Revenaugh, J., & Jordan, T. H. (1991). Mantle layering from scs reverberations: 3. the upper mantle. *Journal of Geophysical Research: Solid Earth*, *96*(B12), 19781–19810.

Revenough, J. (1991). Mantle layering from scs reverberations 4. the lower mantle and core-mantle boundary. *J. geophys. Res.*, *96*, 19811–19824.

Ritsema, J., Deuss, A., van Heijst, H., & Woodhouse, J. (2011). S40rts:a degree-40 shear-velocity model for the mantle from new rayleigh wave dispersion, teleseismic traveltime and normal-mode splitting function measurements. , *184(3)*, 1223-1236.

Schmerr, N., Garnero, E., & McNamara, A. (2010). Deep mantle plumes and convective upwelling beneath the pacific ocean. *Earth and Planetary Science Letters*, *294*(1-2), 143–151.

Shearer, P. M. (2000). Upper mantle seismic discontinuities. *GEOPHYSICAL MONOGRAPH-AMERICAN GEOPHYSICAL UNION*, *117*, 115–132.

Souriau, A. (2007). Deep earth structure-the earth's cores. *Treatise on Geophysics, 1, Seismology and Structure of the Earth*, 655–693.

Tromp, J. (2015). 1.07-theory and obeservations-forward modeling and synthetic seismograms, 3d numerical methods. *Treatise on Geophysics*, 231–251.

Wilson, D., Ringler, A., Storm, T., Hutt, C., & Gee, L. (2013). The importance of removing

seismic sensor instrument response. In *Agu fall meeting abstracts* (Vol. 2013, pp. S42A–04).

Zheng, Z., Ventosa, S., & Romanowicz, B. (2015). High resolution upper mantle discontinuity images across the pacific ocean from ss precursors using local slant stack filters. *Geophysical Journal International*, *202*(1), 175–189.